Supplementary Information: A mathematical model of the circadian clock and drug pharmacodynamics to optimize irinotecan administration timing in colorectal cancer

Janina Hesse[1,2,†], Julien Martinelli[3,4,5†], Ouda Aboumanify[2,6,†], Annabelle Ballesta[3,4,*], Angela Relógio[1,2,6,*]

[1]Institute for Systems Medicine, Department of Human Medicine, MSH Medical School Hamburg – University of Applied Sciences and Medical University, Hamburg 20457, Germany
[2]Institute for Theoretical Biology (ITB), Charité - Universitätsmedizin Berlin, corporate member of Freie Universität Berlin, Humboldt - Universität zu Berlin, and Berlin Institute of Health, Berlin 10117, Germany
[3]INSERM U900, Saint-Cloud, France; Institut Curie, Saint Cloud, France; Paris Saclay University, France; MINES ParisTech, CBIO - Centre for Computational Biology, PSL Research University, Paris, France
[4]UPR 'Chronotherapy, Cancers and Transplantation', Faculty of Medicine, Paris Saclay University, Campus CNRS, 7 rue Guy Moquet, 94800 Villejuif, France
[5]Lifeware Group, Inria Saclay Ile-de-France, Palaiseau, 91120, France
[6]Molecular Cancer Research Center (MKFZ), Medical Department of Hematology, Oncology, and Tumor Immunology, Charité - Universitätsmedizin Berlin, corporate member of Freie Universität Berlin

† These authors contributed equally to this work
∗ Correspondence: annabelle.ballesta@inserm.fr and angela.relogio@charite.de, angela.relogio@medicalschool-hamburg.de

Contents

1 Quantitative core-clock model

1.1 Derivation of the quantitative core-clock model from Relógio *et al.*

1.1.1 The model of Relógio *et al.*

We started from the model of Relógio *et al.* [1], for which a graphical description is provided in **Fig. 1b** of the main text. In this model, paralogs and isoforms are merged into global species, e.g. *Cry* = *Cry1* + *Cry2*. In what follows, we will use the notations adopted in Relógio *et al.* [1] for the parameters and variables. In section 1.1, we describe the changes in model structure that we have done.

1.1.2 Simplification of the PER/CRY loop

The model of Relógio *et al.* [1] contains two parallel PER/CRY loops which account for the fact that PER proteins may exist in phosphorylated or unphosphorylated forms. Considering the lack of quantitative data on PER phosphorylation, we simplified the PER/CRY loop by merging phosphorylated and unphosphorylated species. The new variables refer to the total amount of PER proteins and are defined as:

- $\mathrm{PER}_C^{tot} \leftarrow \mathrm{PER}_C^* + \mathrm{PER}_C$ $(z_2 \leftarrow z_2 + z_3)$
- $\mathrm{PER/CRY}_C^{top} \leftarrow \mathrm{PER^*/CRY}_C + \mathrm{PER/CRY}_C$ $(z_4 \leftarrow z_4 + z_5)$
- $\mathrm{PER/CRY}_N^{top} \leftarrow \mathrm{PER^*/CRY}_N + \mathrm{PER/CRY}_N$ $(x_2 \leftarrow x_2 + x_3)$

Writing the ODEs for these three new variables results in:

$$\begin{aligned}\frac{d(PER_C^* + PER_C)}{dt} &= \frac{d(z_2+z_3)}{dt} \\ &= k_{p_1}y_1 + k_{d_{z_5}}z_5 + k_{d_{ph_{z_3}}}z_3 - k_{f_{z_5}}z_1z_2 - k_{ph_{z_2}}z_2 - d_{z_2}z_2 \\ &+ k_{ph_{z_2}}z_2 + k_{d_{z_4}}z_4 - k_{d_{ph_{z_3}}}z_3 - k_{f_{z_4}}z_1z_3 - d_{z_3}z_3\end{aligned}$$

$$\begin{aligned}\frac{d(PER^*/CRY_C + PER/CRY_C)}{dt} &= \frac{d(z_4+z_5)}{dt} \\ &= k_{f_{z_5}}z_1z_2 + k_{f_{z_4}}z_1z_3 + k_{e_{x_2}}z_2 + k_{e_{x_3}}x_3 \\ &- k_{i_{z_4}}z_4 - k_{i_{z_5}}z_5 - k_{d_{z_4}}z_4 \\ &- k_{d_{z_5}}z_5 - d_{z_4}z_4 - d_{z_5}z_5\end{aligned}$$

$$\begin{aligned}\frac{d(PER^*/CRY_N + PER/CRY_N)}{dt} &= \frac{d(x_2+x_3)}{dt} \\ &= k_{i_{z_4}}z_4 + k_{i_{z_5}}z_5 - k_{e_{x_2}}x_2 - k_{e_{x_3}}x_3 \\ &- d_{x_2}x_2 - d_{x_3}x_3\end{aligned}$$

The phosphorylation parameters $k_{d_{ph_{z_3}}}$ and $k_{ph_{z_2}}$ naturally disappear. The right hand sides of these three ODEs can be re-written in terms of the new variables z_2+z_3, z_4+z_5 and x_2+x_3 by assuming equal parameters for PER phosphorylated and unphosphorylated forms for a given reaction (e.g. nuclear transport, protein degradation, ...). According to the parameter table provided in Relógio *et al.* [1], this is a reasonable assumption. For each reaction, the new parameter was set equal to the mean of parameters obtained in Relógio *et al.* [1] for phosphorylated and unphosphorylated PER proteins, as an initial guess for parameter estimation.

1.1.3 Removal of cytoplasmic complexes degradation parameters

Equations for CLOCK/BMAL and PER/CRY cytoplasmic complexes originally included both a term for complex dissociation into CLOCK, BMAL and PER, CRY free proteins and for complex degradation (i.e. immediate disappearance). These two redundant terms induced problems of model identifiability as there is no available data on any of those two molecular events taken separately, which would allow for reliable parameter estimation. Hence, degradation parameters for the complexes in the cytoplasm were removed. This is equivalent to assuming that the complex needs first to dissociate before the proteins can be degraded.

1.1.4 Refining the CLOCK/BMAL subnetwork

The proven action of CLOCK/BMAL on the expression of genes involved in the irinotecan network implies that the variable CLOCK/BMAL$_N$ is an important exit point from the circadian clock model to the irinotecan network [2, 3]. Therefore, particular attention must be paid to faithfully modelling the dynamics of CLOCK/BMAL nuclear level. Next, while the inital clock model did not explicitly represent *Clock* for the reason that it was found arrhythmic in the SCN [4], the argument does not hold in other tissues such as the liver [5]. For these reasons, we decided to extend the original clock model and included the *Clock* gene as a state variable. *Clock* transcription is regulated through RORE elements family [6] so that ROR and REV-ERB were assumed to act on its transcription, respectively in a positive and negative manner. The cytoplasmic protein CLOCK$_C$ dimerizes in the cytoplasm with BMAL$_C$ [7, 8]. CLOCK/BMAL$_C$ then translocates to the nucleus and becomes the variable CLOCK/BMAL$_N$. We assumed that BMAL nuclear protein level was negligible as it has been observed that BMAL and CLOCK nuclear protein expressions share the same circadian phase and amplitude, suggesting that both species exist majoritarily in complexed forms [9].

1.1.5 Accounting for the cytoplasm/nucleus volume ratio in shuttling dynamics

The mathematical model in Relógio *et al.* [1] did not focus on cellular compartmentalization, and thus potential different volumes for nucleus vs cytoplasm were not considered. This difference can be very large as the fraction of the total cell volume that occupies the nucleus is approximately equal to 10% in mammalian cells (see bionumbers[1]). Thus, the equation terms representing the transport between the cytoplasm and the nucleus need to be scaled to ensure the conservation of the total species quantity (e.g. for nuclear import, what leaves the cytoplasm should be equal to what enters the nucleus). We chose to only modify the equations of the cytoplasm compartment in which all nuclear transport terms are multiplied by the cytoplasm/nucleus volume ratio:

$$\frac{dz_6}{dt} = k_{p_3} y_3 - \frac{v_c}{v_n} k_i z_6 - d_{z_6} z_6$$

1.2 Mathematical description of the quantitative core-clock model

1.2.1 List of variables

Supplementary Table 1 lists the state variables of the core-clock model.

1.2.2 Model equations

CLOCK/BMAL$_C$

$$\frac{dz_9}{dt} = k_{f_{z_9}} z_8 z_5 + \frac{v_c}{v_n} k_{e_{x_1}} x_1 - \frac{v_c}{v_n} k_{i_{z_9}} z_9 - k_{d_{z_9}} z_9 \tag{1.1}$$

CLOCK/BMAL$_N$

$$\frac{dx_1}{dt} = k_{i_{z_9}} z_9 - k_{e_{x_1}} x_1 - d_{x_1} x_1 \tag{1.2}$$

[1] https://bionumbers.hms.harvard.edu/bionumber.aspx?id=113848&ver=0&trm=cytoplasm+nucleus+ratio&org=

Variable name	Species name
x_1	CLOCK/BMAL$_N$
x_2	PER/CRY$_N^{tot}$
x_5	REV-ERB$_N$
x_6	ROR$_N$
y_1	*Per*
y_2	*Cry*
y_3	*Rev-Erb*
y_4	*Ror*
y_5	*Bmal*
y_6	*Clock*
z_1	CRY$_C$
z_2	PER$_C^{tot}$
z_4	PER/CRY$_C^{tot}$
z_5	CLOCK$_C$
z_6	REV-ERB$_C$
z_7	ROR$_C$
z_8	BMAL$_C$
z_9	CLOCK/BMAL$_C$

Supplementary Table 1: List of state variables of the core-clock model.

CLOCK$_C$

$$\frac{dz_5}{dt} = k_{p_6} y_6 + k_{d_{z_9}} z_9 - k_{f_{z_9}} z_8 z_5 - d_{z_5} z_5 \tag{1.3}$$

Rev-Erb

$$\frac{dy_3}{dt} = V_{3_{\max}} \frac{1 + g\left(\frac{x_1}{k_{t_3}}\right)^b}{1 + \left(\frac{x_2}{k_{i_3}}\right)^c \left(\frac{x_1}{k_{t_3}}\right)^b + \left(\frac{x_1}{k_{t_3}}\right)^b} - d_{y_3} y_3 \tag{1.4}$$

Ror

$$\frac{dy_4}{dt} = V_{4_{\max}} \frac{1 + h\left(\frac{x_1}{k_{t_4}}\right)^b}{1 + \left(\frac{x_2}{k_{i_4}}\right)^c \left(\frac{x_1}{k_{t_4}}\right)^b + \left(\frac{x_1}{k_{t_4}}\right)^b} - d_{y_4} y_4 \tag{1.5}$$

REV-ERB$_C$

$$\frac{dz_6}{dt} = k_{p_3} y_3 - \frac{v_c}{v_n} k_{i_{z_6}} z_6 - d_{z_6} z_6 \tag{1.6}$$

ROR$_C$

$$\frac{dz_7}{dt} = k_{p_4} y_4 - \frac{v_c}{v_n} k_{i_{z_7}} z_7 - d_{z_7} z_7 \tag{1.7}$$

REV-ERB$_N$

$$\frac{dx_5}{dt} = k_{i_{z_6}} z_6 - d_{x_5} x_5 \tag{1.8}$$

ROR_N

$$\frac{dx_6}{dt} = k_{i_{z_7}} z_7 - d_{x_6} x_6 \tag{1.9}$$

Clock

$$\frac{dy_6}{dt} = V_{6_{\max}} \frac{1 + j\left(\frac{x_6}{k_{t_6}}\right)^b}{1 + \left(\frac{x_5}{k_{i_6}}\right)^c + \left(\frac{x_6}{k_{t_6}}\right)^b} - d_{y_6} y_6 \tag{1.10}$$

Bmal

$$\frac{dy_5}{dt} = V_{5_{\max}} \frac{1 + i\left(\frac{x_6}{k_{t_5}}\right)^b}{1 + \left(\frac{x_5}{k_{i_5}}\right)^c + \left(\frac{x_6}{k_{t_5}}\right)^b} - d_{y_5} y_5 \tag{1.11}$$

BMAL_C

$$\frac{dz_8}{dt} = k_{p_5} y_5 + k_{d_{z_9}} z_9 - k_{f_{z_9}} z_8 z_5 - d_{z_8} z_8 \tag{1.12}$$

Per

$$\frac{dy_1}{dt} = V_{1_{\max}} \frac{1 + a\left(\frac{x_1}{k_{t_1}}\right)^b}{1 + \left(\frac{x_2}{k_{i_1}}\right)^c \left(\frac{x_1}{k_{t_1}}\right)^b + \left(\frac{x_1}{k_{t_1}}\right)^b} - d_{y_1} y_1 \tag{1.13}$$

Cry

$$\frac{dy_2}{dt} = V_{2_{\max}} \frac{1 + d\left(\frac{x_1}{k_{t_2}}\right)^e}{1 + \left(\frac{x_2}{k_{i_2}}\right)^f \left(\frac{x_1}{k_{t_2}}\right)^e + \left(\frac{x_1}{k_{t_2}}\right)^e} \frac{1}{1 + \left(\frac{x_5}{k_{i_{21}}}\right)^{f_1}} - d_{y_2} y_2 \tag{1.14}$$

CRY_C

$$\frac{dz_1}{dt} = k_{p_2} y_2 + k_{d_{z_4}} z_4 - k_{f_{z_4}} z_1 z_2 - d_{z_1} z_1 \tag{1.15}$$

PER_C^{tot}

$$\frac{dz_2}{dt} = k_{p_1} y_1 + k_{d_{z_4}} z_4 - k_{f_{z_4}} z_1 z_2 - d_{z_2} z_2 \tag{1.16}$$

$\mathrm{PER/CRY}_C^{tot}$

$$\frac{dz_4}{dt} = k_{f_{z_4}} z_1 z_2 + \frac{v_c}{v_n} k_{e_{x_2}} x_2 - \frac{v_c}{v_n} k_{i_{z_4}} z_4 - k_{d_{z_4}} z_4 \tag{1.17}$$

PER/CRY$_N^{tot}$

$$\frac{dx_2}{dt} = k_{i_{z_4}} z_4 - k_{e_{x_2}} x_2 - d_{x_2} x_2 \tag{1.18}$$

1.2.3 List of model parameters of the core-clock model

Parameter	Name	Liver	SW480	SW620
Degradation rates for nuclear proteins or nuclear protein complexes [hour^{-1}]				
d_{x_1}	CLOCK/BMAL	0.2565	0.1017	0.1806
d_{x_2}	PER/CRY$_N^{tot}$	0.1267	0.7392	0.3232
d_{x_5}	REV-ERB$_N$	1.7383	2.4484	0.1183
d_{x_6}	ROR$_N$	1.3175	0.6792	1.6102
Degradation rates for mRNAs [hour^{-1}]				
d_{y_1}	*Per*	0.4977	0.2913	1.3323
d_{y_2}	*Cry*	0.4194	0.134	0.0347
d_{y_3}	*Rev-Erb*	0.6743	2.4956	2.2398
d_{y_4}	*Ror*	0.2352	0.035	0.0312
d_{y_5}	*Bmal*	0.3198	2.5	1.9949
d_{y_6}	*Clock*	0.3235	0.3381	0.2074
Degradation rates for cytoplasmic proteins [hour^{-1}]				
d_{z_1}	CRY$_C$	0.3125	2.4994	2.9975
d_{z_2}	PER$_C$	0.0662	0.0409	0.0364
d_{z_5}	CLOCK$_C$	0.6229	1.6832	2.3992
d_{z_6}	REV-ERB$_C$	0.3378	0.0414	0.032
d_{z_7}	ROR$_C$	0.7913	0.1356	0.1363
d_{z_8}	BMAL$_C$	0.3014	1.1466	2.6224
Reaction rates for complex formation [nmol$\times L^{-1}\times$hours^{-1}]				
$k_{f_{z_9}}$	CLOCK/BMAL$_C$	0.0657	0.0169	0.0563
$k_{f_{z_4}}$	PER/CRY$_C^{tot}$	0.0318	0.0257	0.0341
Reaction rates for complex dissociation [hours^{-1}]				
$k_{d_{z_9}}$	CLOCK/BMAL$_C$	0.279	0.6536	2.9995
$k_{d_{z_4}}$	PER/CRY$_C^{tot}$	0.021	0.3111	0.3573
Transcription rates [nmol$\times L^{-1}\times$ hours^{-1}]				
$V_{1_{\max}}$	*Per*	0.1431	2.5165	5.5144
$V_{2_{\max}}$	*Cry*	0.0496	0.0523	0.1499
$V_{3_{\max}}$	*Rev-Erb*	0.0079	0.0267	0.0057
$V_{4_{\max}}$	*Ror*	0.0393	0.0004	0.0018
$V_{5_{\max}}$	*Bmal*	0.0027	0.1713	0.0203
$V_{6_{\max}}$	*Clock*	0.0027	0.0073	0.0022
Activation/inhibition rates [nmol$\times L^{-1}$]				
k_{t_1}	*Per*-activation rate	0.066	0.0065	0.0189
k_{i_1}	*Per*-inhibition rate	1.1912	0.5495	0.5672
k_{t_2}	*Cry*-activation rate	241.2015	18.7184	22.6995
k_{i_2}	*Cry*-inhibition rate	0.0223	0.0021	0.0016
$k_{i_{21}}$	*Cry*-inhibition rate	11.5034	15.0881	19.7684
k_{t_3}	*Rev-Erb*-activation rate	0.0716	0.0186	0.0054
k_{i_3}	*Rev-Erb*-inhibition rate	14.9091	15.6085	39.5099
k_{t_4}	*Ror*-activation rate	4.6929	10.2838	45.7059
k_{i_4}	*Ror*-inhibition rate	0.0012	0.0015	0.0023

k_{t_5}	*Bmal*-activation rate	18.4408	10.1313	3.5061
k_{i_5}	*Bmal*-inhibition rate	10.5553	15.1897	98.7832
k_{t_6}	*Clock*-activation rate	0.01593	0.4121	1.1779
k_{i_6}	*Clock*-inhibition rate	46.9265	31.3405	165.0875
	Transcription fold activation (dimensionless)			
a	*Per*	30.0384	1.6157	4.0879
d	*Cry*	6.0566	107.1115	94.8115
g	*Rev-Erb*	198.347	22.2163	32.5303
h	*Ror*	9.7537	195.1387	120.3863
i	*Bmal*	12	12	12
j	*Clock*	3.3507	17.8863	11.5117
	Production rates [molecules $\times$ mRNA$^{-1}\times$ hour^{-1}]			
k_{p_1}	PER_C^{tot}	384.9242	17175.9753	4058.6511
k_{p_2}	CRY_C	469.6348	13313.783	9622.3143
k_{p_3}	REV-ERB_C	2695.93	33397.5015	78769.4987
k_{p_4}	ROR_C	338.6881	18.1801	161.066
k_{p_5}	BMAL_C	803.5155	1706.2512	16006.2689
k_{p_6}	CLOCK_C	288.4416	2047.4364	2858.2369
	Import/Export rates [hour^{-1}]			
$k_{i_{z_4}}$	PER/CRY_C^{tot}	0.03407	0.0549	0.0506
$k_{i_{z_6}}$	REV-ERB_C	0.4057	0.0135	0.0018
$k_{i_{z_7}}$	ROR_C	0.0011	0.0044	0.0113
$k_{i_{z_9}}$	CLOCK/BMAL_C	0.001	0.0011	0.0012
$k_{e_{x_1}}$	CLOCK/BMAL_N	0.4025	0.2495	0.9313
$k_{e_{x_2}}$	PER/CRY_N^{tot}	0.00005	0.003	0.0014
	Hill coefficients of transcription (dimensionless)			
b	activation	8	6.1184	7.5482
c	inhibition	4.5568	6.425	5.8353
e	*Cry*-activation	5.1910	7.9585	5.2423
f	*Cry*-inhibition	7.9525	7.9968	6.5434
f_1	*Cry*-inhibition	1	7.9587	3.5099
	Volume proportion (dimensionless)			
v_c	cytoplasm	0.93	0.8	0.8
v_n	nucleus	0.07	0.2	0.2

Supplementary Table 2: List of parameters and optimal values for each dataset.

Hill coefficients can be related to the number of boxes in the promoter of the target gene and should therefore remain to low values (e.g. 3 for Rev-Erb [10]). However, the transcription term in the equations is only semi-mechanistic and encompasses all molecular events from the activation of transcription regulators (e.g. BMAL1/CLOCK) in the nucleus to the production of mRNA molecules ultimately reaching the cytoplasm. Thus, such term can implicitly model more complex networks such as activation cascades [11], which may explain why Hill coefficients may present higher values than expected for few genes. When fitting the mouse liver clock data, constraining all Hill coefficients to lower values (i.e. below 5) did not yield satisfactory results in terms of model fit. Therefore, the coefficients were constrained between 1 and 8 to allow larger values. A similar finding is reported in [12].

1.3 Model calibration

1.3.1 Gene and protein circadian expression datasets and their preprocessing

Datasets reported in Narumi *et al.* [5] were used to estimate parameters of the quantitative core-clock model in mouse liver. These are time series of gene and protein circadian expression for the core-clock species, measured in the liver of C57BL6 male mice synchronized with 12 hours of light and 12 hours of darkness. Gene expression data was obtained through RT-PCR while the proteomics data were obtained through a novel mass spectrometry workflow allowing for the quantification of protein

concentrations. Both datasets had a time resolution of 4 hours up to 48h (resp. 24h) for the genomics (resp. proteomics) study. Two mice were analyzed per time point. Our data processing workflows for genes and proteins is summarized below.

Genes:

- Sum every paralog into one species (e.g. *Per* = *Per1* + *Per2* + *Per3*) for each model variable, if need be
- Multiply every expression by the intracellular concentration of the reference gene *Tbp*. *Tbp* concentration was estimated using the value reported in Schmidt and Schibler [13] expressed in molecules/cell. This quantity was converted from molecules/cell into mol/L by dividing by the Avogadro number and dividing by the cell volume assumed to be equal to 1pL.

Proteins:

- Average the concentration of all identified peptides for each protein present in the model.
- Sum every paralog-induced proteins into one species (e.g. PER = PER1 + PER2 + PER3).
- Convert values from molecules/cell to mol/L by dividing by the Avogadro number and dividing by the cell volume assumed to be equal to 1pL.

In the case of proteins, the data acquisition technique provided us with total intracellular protein amounts so that the mapping to the outputs of the clock model was not straightforward. Indeed, the model contains variables in different compartments (nucleus, cytoplasm) and under different forms (free or in complex). Hence, protein data was mapped to aggregated variables for BMAL, CLOCK, PER, CRY, REV-ERB and ROR which were defined as follows:

$$BMAL_{tot} = \frac{v_c}{v_t} BMAL_C + \frac{v_c}{v_t} CLOCK/BMAL_C + \frac{v_n}{v_t} CLOCK/BMAL_N \tag{1.19}$$

$$CLOCK_{tot} = \frac{v_c}{v_t} CLOCK_C + \frac{v_c}{v_t} CLOCK/BMAL_C + \frac{v_n}{v_t} CLOCK/BMAL_N \tag{1.20}$$

$$PER_{tot} = \frac{v_c}{v_t} PER_C + \frac{v_c}{v_t} PER/CRY_C + \frac{v_n}{v_t} PER/CRY_N \tag{1.21}$$

$$CRY_{tot} = \frac{v_c}{v_t} CRY_C + \frac{v_c}{v_t} PER/CRY_C + \frac{v_n}{v_t} PER/CRY_N \tag{1.22}$$

$$REV\text{-}ERB_{tot} = \frac{v_c}{v_t} REV\text{-}ERB_C + \frac{v_n}{v_t} REV\text{-}ERB_N \tag{1.23}$$

$$ROR_{tot} = \frac{v_c}{v_t} ROR_C + \frac{v_n}{v_t} ROR_N \tag{1.24}$$

where v_c (resp. v_n) is the cytoplasm (resp. nucleus) volume and v_t the total cell volume, so that $v_t = v_c + v_n$.

The nuclear amount of free proteins were assumed to be negligible since BMAL and CLOCK nuclear protein expressions shared the same circadian phase and amplitude, suggesting that both species exist majoritarily in complexed forms [9].

1.3.2 Derivation of a fully quantitative model

The previous clock model by Relógio *et al.* was expressed in arbitrary units (a.u.), due to the lack of absolutely quantitative information. The objective of this study was to design a fully quantitative model, able to predict not only the circadian phase and amplitude of genes and proteins, but also their mean levels, which could be of crucial importance in the context of pharmacology, where an optimal dose is sought for. Starting from the initial model, we have derived a first quantitative model through the following pipeline.

Let x be a model variable in a.u. and let x' be the scaled variable in **mol/L** s.t.

$$x' = x \times \frac{x^D_{\max}}{x^M_{\max}} = x \times x_{\max}$$

where $x^D_{\max}$ is the maximum value from the genes and protein data of Narumi *et al.* [5], expressed in mol/L, and $x^M_{\max}$ the maximum value in the simulation of the original model, thus expressed in a.u.. Then $x \in [0, x^M_{\max}]$ and $x' \in [0, x^D_{\max}]$. This change of variable induces a scaling on the parameters which provided us with new parameter estimates that were used as initial guess in the parameter estimation procedure. For instance, scaling the equation for z_6 results in:

$$\frac{dz_6}{dt} = k_{p_3} y_3 - \frac{v_c}{v_n} k_{iz6} z_6 - d_{z_6} z_6$$

$$\frac{dz'_6}{dt} = k_{p_3} \frac{z_{6\max}}{y_{3\max}} y'_3 - \frac{v_c}{v_n} k_{iz6} z'_6 - d_{z_6} z'_6$$

This showed that only the parameter k_{p_3} needed to be scaled whereas the parameters $k_{i_{z_6}}$ and $k_{d_{z_6}}$ were unchanged by the change of model unit. Scaled parameters belong to the following families: complex formation rates, transcription rates, activation/inhibition rates and production rates.

1.3.3 Reducing the number of free parameters using clock protein expression in *Bmal1*$^{-/-}$ mice

The article of Narumi *et al.* [5] from which circadian genomics and proteomics data were used here for parameter estimation also featured data in *Bmal1* KO conditions. Clock protein concentrations were quantified in the liver of *Bmal1*$^{-/-}$ mice sacrificed at CT4 and CT16. These datasets were used to further constrain the model parameter estimation as follows. In a nutshell, three transcription parameters $V_{\max}$ could be expressed with respect to these datasets and to the other parameters of the model, thus leading to a reduction of the number of parameters to estimate.

Knockout of *Bmal1* is known to result in an arrhythmic circadian clock [14] , as the transcription factor CLOCK/BMAL, a key component of the two main negative feedback loop, is absent. The obtained protein concentrations time series are flat and we can reasonably assume that the system is at equilibrium. The equation Eq. 1.4 for *Rev-Erb* mRNA level (y_3), accounting for the absence of BMAL, hence of CLOCK/BMAL, gives at steady state:

$$\begin{aligned} \frac{dy_3}{dt} &= 0 \\ \Leftrightarrow V_{3_{\max}} - d_{y_3} y_3 &= 0 \\ \Leftrightarrow \frac{V_{3_{\max}}}{d_{y_3}} &= y_3 \end{aligned}$$

Plugging this expression into Eq. 1.6 for REV-ERB$_C$ (z_6):

$$\begin{aligned} k_{p_3} \frac{V_{3_{\max}}}{d_{y_3}} - \frac{v_c}{v_n} k_{i_{z_6}} z_6 - d_{z_6} z_6 &= 0 \\ \Leftrightarrow (\frac{v_c}{v_n} k_{i_{z_6}} + d_{z_6}) \frac{d_{y_3}}{k_{p_3}} z_6 &= V_{3_{\max}} \end{aligned}$$

We can now use the Rev-erb protein level experimentaly observed in KO mice, we have $Rev^{DataKO} = v_c z_6 + v_n x_5$. Eq. 1.8 for REV-ERB$_N$ (x_5) at steady state gives $k_{i_{z_6}} z_6 - d_{x_5} x_5 = 0$ which is used to express x_5 in terms of z_6. Finally,

$$V_{3_{\max}} = (\frac{v_c}{v_n} k_{i_{z_6}} + d_{z_6}) \frac{d_{y_3}}{k_{p_3}} \frac{Rev^{DataKO}}{v_c + v_n \frac{k_{i_{z_6}}}{d_{x_5}}}, \tag{1.25}$$

which results in an equation for $V_{3_{\max}}$ only depending on the KO data and on the parameters of the model. The procedure is exactly the same for $V_{4_{\max}}$ which leads to the following formula:

$$V_{4_{\max}} = (\frac{v_c}{v_n} k_{i_{z_7}} + d_{z_7}) \frac{d_{y_4}}{k_{p_4}} \frac{Ror^{DataKO}}{v_c + v_n \frac{k_{i_{z_7}}}{d_{x_6}}} \tag{1.26}$$

For $V_{6_{\max}}$, at steady state, the equation for CLOCK mRNA (y_6) becomes:

$$V_{6_{\max}} \frac{1 + j \left(\frac{x_6}{k_{t_6}}\right)^b}{1 + \left(\frac{x_5}{k_{i_6}}\right)^c + \left(\frac{x_6}{k_{t_6}}\right)^b} = d_{y_6} y_6$$

From the above computations,

$$x_5 = \frac{k_{iz_6}}{d_{x_5}} \frac{Rev^{DataKO}}{v_c + v_n \frac{k_{i_{z_6}}}{d_{x_5}}}$$

Similarly, an expression for x_6 can be derived as:

$$x_6 = \frac{k_{iz_7}}{d_{x_6}} \frac{ROR^{DataKO}}{v_c + v_n \frac{k_{i_{z_7}}}{d_{x_6}}}$$

Hence, the Hill-function-like term is then entirely determined and will be denoted H. Using Eq. 1.2.2, y_6 can be expressed in terms of z_5:

$$\frac{V_{6_{\max}}}{d_{y_6}} k_{p_6} H = d_{z_5} z_5$$

We assumed that the observed CLOCK protein expression level in KO mice only corresponded to cytoplasmic CLOCK (z_5), as co-expression experiments performed in Kondratov *et al.* [15] showed a reduced nuclear fraction of CLOCK to the nucleus in the absence of BMAL1. Hence we have: $Clock^{DataKO} = z_5$ and finally:

$$V_{6_{\max}} = \frac{d_{y_6}}{k_{p_6} H} d_{z_5} Clock^{DataKO} \tag{1.27}$$

For $V_{1_{\max}}$ and $V_{2_{\max}}$, the complexation of PER^*_C and CRY_C introduces additional variables as well as non linear terms in the protein equations. In this case, the existence of an equation linking $V_{1_{\max}}$ and $V_{2_{\max}}$ to other parameters becomes conditional to the satisfaction of some stability criterion, leading to cumbersome computations in an optimization pipeline, therefore these parameters remained estimated. Similarly, $V_{5_{\max}}$ which corresponds to *Bmal* transcription, could not be derived this way.

1.3.4 Fitting the circadian time series through a least square approach

The first part of the parameter fitting procedure aimed to reproduce the circadian genomics and proteomics time-resolved data from Narumi *et al.* [5]. In order to do so, we defined a cost function $L(\theta)$ as the sum of squared residuals across species $s \in S$, divided by the maximum value of a species's concentration along time:

$$L(\theta) = \sum_{s\in S}\left(\sum_{t_i\in\mathcal{T}_g}\sum_{j\in\mathcal{J}}\left(\frac{y^{(s)}_{t_i,j}-\hat{y}^{(s)}_{t_i,j}(\theta)}{y^{(s)}_{\max}}\right)^2+\sum_{t_i\in\mathcal{T}_p}\sum_{j\in\mathcal{J}}\left(\frac{Y^{(s)}_{t_i,j}-\hat{Y}^{(s)}_{t_i,j}(\theta)}{Y^{(s)}_{\max}}\right)^2\right) \tag{1.28}$$

where y (resp. Y) is the mRNA data (resp. protein data). $\hat{y}$ is the model simulation for the mRNA expression, $\hat{Y}$ refers to the convex combination of protein species defined in Eq. 1.3.1 whose model simulation will be compared to a protein Y in the data. $\mathcal{T}_g = \{0, 4, 8, \ldots, 44\}$ (resp. $\mathcal{T}_p = \{0, 4, 8, \ldots, 24\}$) are the circadian times of data measurement for the mRNAs (resp. proteins), $\mathcal{J} = \{1, 2\}$ is the number of the replica. Finally, for each species $s \in S, y^{(s)}_{\max} = \max_{\substack{t_i\in\mathcal{T}_g\\ j\in J}} y^{(s)}_{t_i,j}$ and $Y^{(s)}_{\max} = \max_{\substack{t_i\in\mathcal{T}_p\\ j\in J}} Y^{(s)}_{t_i,j}$

Dividing by the maximum values ensures that genes and proteins have the same importance in the cost function even though their mean levels are different by several orders of magnitude.

1.3.5 Constraining the parameter estimation with additional biological knowledge

It is well known in systems biology that fitting even large amounts of data with a model including numerous parameters can end up in many adequate parameter sets [16]. Therefore, we used biological knowledge as a way to constraint the parameter estimation.

The first type of constraints considered acts directly on the parameter search interval to ensure biological coherence, based on experimental data. The transcription rates of $\approx$ 5,000 genes were measured by Schwanhäusser *et al.* [17]. Using the maximum of these rates μ, transcription rates of the model can be upper bounded.

Indeed, considering for instance Eq. 1.4 for *Rev-Erb*:

$$\begin{aligned}\frac{dy_3}{dt} &= V_{3_{\max}}\frac{1+g\left(\frac{x_1}{k_{t_3}}\right)^v}{1+\left(\frac{x_2}{k_{i_3}}\right)^w\left(\frac{x_1}{k_{t_3}}\right)^v+\left(\frac{x_1}{k_{t_3}}\right)^v}-d_{y_3}y_3\\ \implies \lim_{\substack{x_1\to+\infty\\ x_2\to 0}}\frac{dy_3}{dt} &= gV_{3_{\max}}-d_{y_3}y_3\end{aligned}$$

This gives us $gV_{3_{\max}} \leqslant \mu$. Similarly we can derive a constraint for each other gene of the model. In practice we set $\mu = 5\text{nmol} \times L^{-1} \times \text{hours}^{-1}$ for each gene.

Due to their connection with half-lives, degradation parameters can also be constrained so as to represent plausible half-lives. Then again, the data reported by Schwanhäusser *et al.* [17] can be useful. We then chose to bound degradation parameters between $[10^{-4}, 3]$

The second type of constraints included act on the model outputs, constraining them to a desired behavior. The protein data acquisition technique provided total protein amount but information on the relative quantities of proteins either free or in complexe was missing. Using co-immunoprecipitation data from Zheng *et al.* [7] and immunodepletion from Aryal *et al.* [18], we arrived at the final expression to bind the concentration of the complexes.

$$0.15\ CLOCK_{tot} \leqslant v_c CLOCK/BMAL_C + v_n CLOCK/BMAL_N \leqslant 0.85\ CLOCK_{tot}$$
$$PER/CRY_C^{tot} \geqslant 0.5 PER_C^{tot}$$

Where $\text{CLOCK}_{tot} = v_c(\text{CLOCK}_C + \text{CLOCK/BMAL}_C) + v_n\ \text{CLOCK/BMAL}_N$

All these constraints were incorporated in the optimization in such a way that a resample of the parameter vector was initiated whenever any of them was violated, therefore the parameter vector responsible for such constraint violation was discarded.

1.4 Robustness analysis

We assessed the robustness of our model against parameter perturbations in terms of oscillatory behaviour. More precisely, in this case, let $Y = f(\theta)$ be the boolean variable indicating whether or not a model parametrized by a vector θ outputs periodic simulation or not. The parameter vector θ will be slightly perturbed around its base value for each coordinate, and is therefore seen as a random variable. A grid $[0.9 * \theta, 1.1 * \theta]$ is then produced and Y evaluated for up to 100000 samples within that grid. 73% of these evaluations led to periodic simulations.

Sobol sensitivity total order indices were then computed [19]. The total-order-index S_{T_i} measures the contribution of a variable θ_i in the output variance of a variable Y, including all variance caused by θ_i's interactions of any order with the other variables θ_j.

$$S_{T_i} = \frac{E_{\theta \sim i}\left(\mathrm{Var}_{\theta_i}(Y|\theta_{\sim i})\right)}{\mathrm{Var}(Y)}$$

where $\mathrm{Var}(\cdot|\cdot)$ is the conditional variance, and $\theta_{\sim i}$ is the set of all parameters except θ_i.

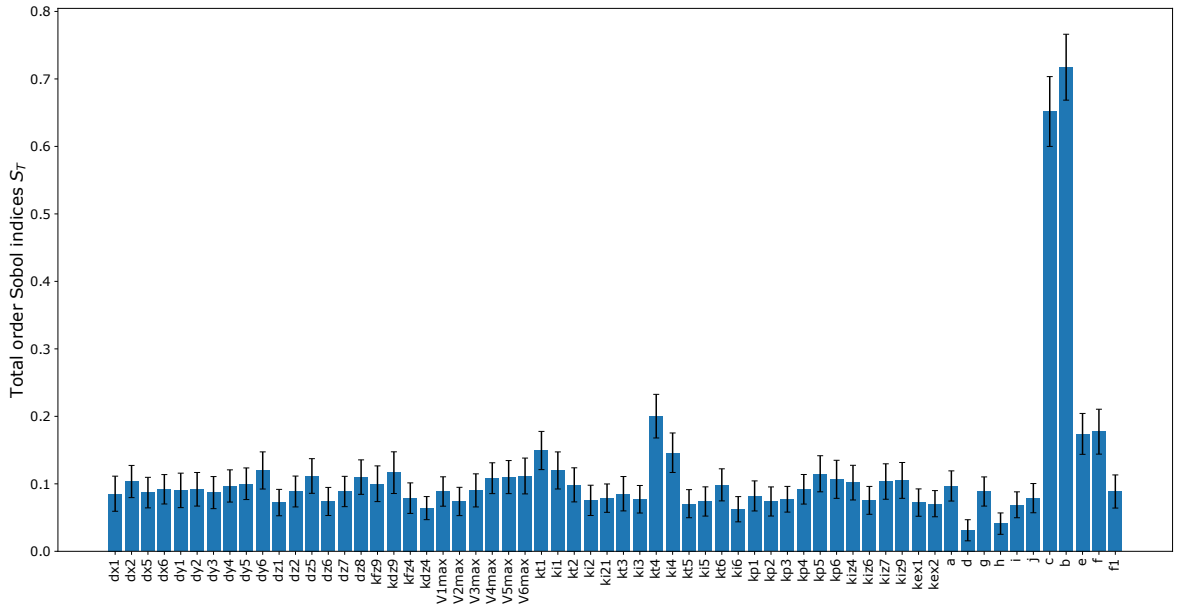

Supplementary Figure 1: Total order Sobol indices for the core-clock model. 100 000 simulations of the model were used for the estimation.

The fact that mutual Hill coefficients b and c produces high values for total order indices was expected as these parameters are present in five equations.

2 Supplementary figures to the core-clock model

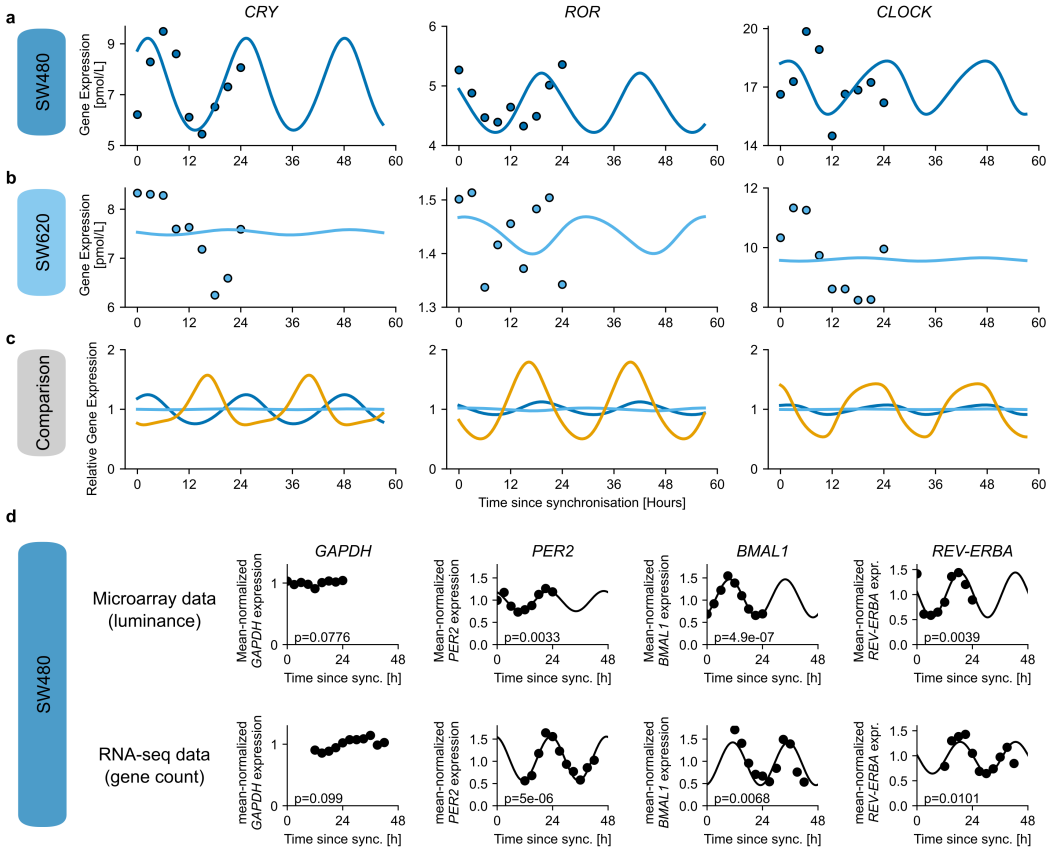

Supplementary Figure 2: **Fit of the core-clock model to cell lines derived from human cancer.** This supplements figure 3 of the main text, showing the remaining genes of the core-clock. **a** Fit (line) and experimental data (dots) for the SW480 cell line and **b** the SW620 cell line. **c** Comparison of the model fit for liver (orange), SW480 (dark blue) and SW620 (sky blue). Bmal1 circadian phases were aligned for mouse liver and SW480 cell line and all gene expression were normalized to the mesor to allow for comparison. **d** Comparison of microarray and RNA-seq time-series data for the reference gene *GAPDH* and the core-clock genes measured for the RT-qPCR data of the SW480 and SW620 cell lines. *GAPDH* is particularly well suited as reference gene as it is expressed at a much higher abundance compared to core-clock genes, and it does not show circadian oscillations, as confirmed by a cosinor analysis with non-significant p-values for *GAPDH*. Experimental mean-normalized measures (dots) with the result from a harmonic regression (lines), using a p-value threshold of p=0.05.

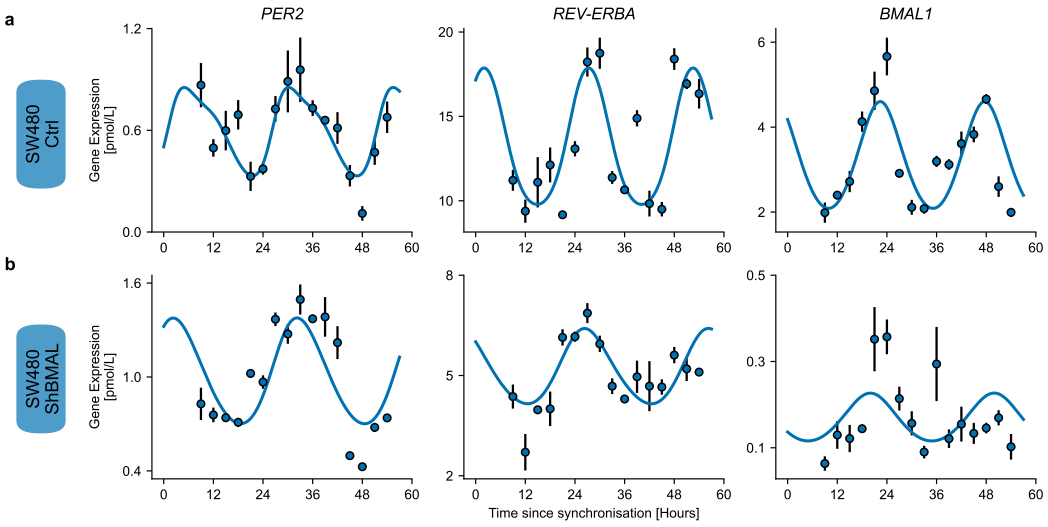

Supplementary Figure 3: **SW480 control and Bmal knock-down can be fitted by similar core-clock models.** **a** Fit of the core-clock model to qRT-PCR data of the SW480 cell line in Ctrl condition, **b** Fit of the core-clock model to qRT-PCR data of the SW480 cell line in shBmal condition, varying only *Bmal1* transcription rate.

3 The clock-irinotecan model

Gene name (A)	Action	Gene name (B)	Reference
CLOCK	**binds to**	BMAL1	[1]
CLOCK:BMAL1	**Activates**	*PER*	[4, 20]
CLOCK:BMAL1	**Activates**	*CRY*	[4, 20]
CLOCK:BMAL1	**Activates**	*ROR*	[4, 20]
CLOCK:BMAL1	**Activates**	*REV-ERB*	[4, 20]
PER	**binds to**	CRY	[21]
PER/CRY	**Inhibits**	CLOCK:BMAL1 transcription	[22]
ROR	**Activates**	*BMAL1*	[23]
REV-ERB	**Inhibits**	*BMAL1*	[23]
REV-ERB	**Inhibits**	*CRY*	[24]
CLOCK:BMAL1	**Activates**	*DBP* (*PAR bZip*)	[25]
CLOCK:BMAL1	**Activates**	*HLF* (*PAR bZip*)	[26]
ROR	**Activates**	*NFIL3* (*E4BP4*)	[26]
REV-ERB	**Inhibits**	*NFIL3* (*E4BP4*)	[26]
CLOCK:BMAL1	**Activates**	*PPARa*	[3]
DBP	**Activates**	*TOP1*	[2]
NFIL3	**Inhibits**	*TOP1*	[2]
CLOCK:BMAL1	**Activates**	*TOP1*	[2]
TOP1	**Inhibits**	*BMAL1*	[27]
NFIL3	**Activates**	*CES2*	[28]
NFIL3	**Inhibits**	*REV-ERB*	[28]
REV-ERB	**Inhibits**	*CES2*	[28]
DBP (PAR bZip)	**Activates**	*ABCC2*	[29]
NFIL3	**Inhibits**	*ABCC2*	[29]
HLF (PAR bZip)	**Activates**	*ABCB1*	[30]
NFIL3	**Inhibits**	*ABCB1*	[30]
PPARa	**Activates**	*UGT1A1*	[31]

Supplementary Table 3: Overview over the connections in the translation-transcription network, with references for experimental reports of the connection from various experimental setups.

The clock-irinotecan model extends the core-clock model from Section 1.2, with the dynamics of *Bmal1* and *Rev-Erb* as stated below, by the interactions as depicted in **Figure 4** of the main text.

The variables and parameters of the core-clock model are used for elements belonging to the core-clock. Additional dynamic variables of the clock-irinotecan model are stated in Supplementary Table 4. For genes only the first letter is uppercase, proteins are set in uppercase, concentrations are denoted with square brackets [.]. For simplicity, the model does not explicitly differentiate between cytosolic and nuclear proteins for irinotecan PK/PD-related genes.

Feedback to the core-clock: Transcription of *Bmal1* and *Rev-Erb*

The transcription of *Bmal1* and *Rev-Erb* is replaced by the following equations, which implement the feedback from *Top1* and *Nfil3*.

Bmal1

$$\frac{\mathrm{d}y_5}{\mathrm{d}t} = V_{5_{\max}} \frac{1 + i\left(\frac{x_6}{k_{t_5}}\right)^b}{1 + \left(\frac{x_5}{k_{i_5}}\right)^c + \left(\frac{x_6}{k_{t_5}}\right)^b} \frac{1}{1 + \left(\frac{[\mathrm{TOP}]}{i_{\mathrm{BmalTop}}}\right)^c} - d_{y_5} y_5 \tag{3.1}$$

Rev-erb

Gene name	Variable name
Bmal1	y_5
Rev-Erb	y_3
Ces2	Ces
Ugt1a1	Ugt
Abcb1	$Abcb$
Abcc	$Abcc$
Pparα	$Ppar$
Top1	Top
PAR bZip	Par
Nfil3	$Nfil$
CES1	CES
UGT1A1	UGT
ABCB1	$ABCB$
ABCC	$ABCC$
PPARα	$PPAR$
TOP1	TOP
PAR bZIP	PAP
NFIL3	$NFIL$

Supplementary Table 4: List of dynamical state variables representing mRNAs and proteins. For the irinotecan-related genes, the model uses the same variable names for mRNA and proteins, the latter in uppercase.

$$\frac{\mathrm{d}y_3}{\mathrm{d}t} = V_{3_{\max}} \frac{1 + g\left(\frac{x_1}{k_{t_3}}\right)^b}{1 + \left(\frac{x_2}{k_{i_4}}\right)^c \left(\frac{x_1}{k_{t_3}}\right)^b + \left(\frac{x_1}{k_{t_3}}\right)^b} \frac{1}{1 + \left(\frac{[\mathrm{NFIL}]}{i_{\mathrm{RevNfil}}}\right)^c} - d_{y_3} y_3 \tag{3.2}$$

3.1 Equations of the network connecting core-clock and irinotecan dynamics

3.1.1 Translation

The protein is degraded and grows by translation, where d_{PROTEIN} is the degradation rate, and r_{PROTEIN} is a translation rate that either describes only the translation of the gene to the cytoplasmic protein (first four variables of Table 1), or both the translation step as well as the import of this protein into the nucleus (last four variables of Table 1).

For the elements of Supplementary Table 4 the step from genes to proteins has the same structure:

$$\frac{\mathrm{d}PROTEIN}{\mathrm{d}t} = r_{\mathrm{PROTEIN}}\, mRNA - d_{\mathrm{PROTEIN}}\, PROTEIN \tag{3.3}$$

3.1.2 Transcription

The transcription of all variables of Supplementary Table 4 and of *Bmal1* and *Rev-Erb* follow dynamics with the following structure:

$$\frac{\mathrm{d}mRNA}{\mathrm{d}t} = V_{\mathrm{mRNA}} \mathbb{T}(mRNA) - d_{\mathrm{mRNA}}\, mRNA, \tag{3.4}$$

where V_{Gene} is the maximal transcription rate of the gene *Gene*, d_{Gene} is the degradation rate of the gene, and $\mathbb{T}(Gene)$ is the transcription function as defined below, that includes the interactions between different elements.

Parameter name	Parameter symbol
transcription function as stated below	$\mathbb{T}(Gene)$
maximal transcription rate of the gene *Gene*	V_{Gene}
degradation rate of the gene *Gene*	d_{Gene}
transcription fold activations	f_{Gene}
activation rates	a_{Gene}
inhibition rates for inhibition by one protein	i_{Gene}
inhibition rate of TOP1 on *Bmal1*	i_{BmalTop}
inhibition rate of NFIL3 on *Rev-Erb*	i_{RevNfil}
activation rate of CLOCK/BMAL on *Top1*	a_{Top}
activation rate of PAR bZIP on *Top1*	a_{TopPar}
inhibition rate of PER/CRY on *Top1*	i_{Top}
inhibition rate of NFIL3 on *Top1*	i_{TopNfil}
Hill coefficient of activation	b
Hill coefficient of inhibition	c
rate of translation* of the protein *PROTEIN*	r_{PROTEIN}
degradation rate of the protein *PROTEIN*	d_{PROTEIN}

Supplementary Table 5: List of model parameters. * For PPARα, TOP1, PAR bZIP and NFIL3, r_{PROTEIN} is the rate of translation and the import of the protein into the nucleus.

Transcription functions For simplicity, the Hill coefficients of transcription for activation and inhibition, b and c, are the same for all equations.

Pparα

$$\mathbb{T}(Ppar) = \frac{1 + f_{\text{Ppar}} \left(\frac{x_1}{a_{\text{Ppar}}}\right)^b}{1 + \left(\frac{x_2}{i_{\text{Ppar}}}\right)^c \left(\frac{x_1}{a_{\text{Ppar}}}\right)^b + \left(\frac{x_1}{a_{\text{Ppar}}}\right)^b} \tag{3.5}$$

PAR bZip

$$\mathbb{T}(Par) = \frac{1 + f_{\text{Par}} \left(\frac{x_1}{a_{\text{Par}}}\right)^b}{1 + \left(\frac{x_2}{i_{\text{Par}}}\right)^c \left(\frac{x_1}{a_{\text{Par}}}\right)^b + \left(\frac{x_1}{a_{\text{Par}}}\right)^b} \tag{3.6}$$

Ugt1a1

$$\mathbb{T}(Ugt) = \frac{1 + f_{\text{Ugt}} \left(\frac{[\text{PPAR}]}{a_{\text{Ugt}}}\right)^b}{1 + \left(\frac{[\text{PPAR}]}{a_{\text{Ugt}}}\right)^b} \tag{3.7}$$

Nfil3

$$\mathbb{T}(Nfil) = \frac{1 + f_{\text{Nfil}} \left(\frac{x_6}{a_{\text{Nfil}}}\right)^b}{1 + \left(\frac{x_5}{i_{\text{Nfil}}}\right)^c + \left(\frac{x_6}{a_{\text{Nfil}}}\right)^b} \tag{3.8}$$

Ces

$$\mathbb{T}(Ces) = \frac{1 + f_{\text{Ces}} \left(\frac{[\text{NFIL}]}{a_{\text{Ces}}}\right)^b}{1 + \left(\frac{x_5}{i_{\text{Ces}}}\right)^c + \left(\frac{[\text{NFIL}]}{a_{\text{Ces}}}\right)^b} \tag{3.9}$$

Abcb1

$$\mathbb{T}(Abcb) = \frac{1 + f_{\text{Abcb}} \left(\frac{[\text{PAR}]}{a_{\text{Abcb}}}\right)^b}{1 + \left(\frac{[\text{NFIL}]}{i_{\text{Abcb}}}\right)^c + \left(\frac{[\text{PAR}]}{a_{\text{Abcb}}}\right)^b} \tag{3.10}$$

Abcc

$$\mathbb{T}(Abcc) = \frac{1 + f_{\text{Abcc}} \left(\frac{[\text{PAR}]}{a_{\text{Abcc}}}\right)^b}{1 + \left(\frac{[\text{NFIL}]}{i_{\text{Abcc}}}\right)^c + \left(\frac{[\text{PAR}}{a_{\text{Abcc}}}\right)^b} \tag{3.11}$$

Top1

$$\mathbb{T}(Top) = \frac{1 + f_{\text{Top}} \left(\frac{x_1}{a_{\text{Top}}}\right)^b}{1 + \left(\frac{x_2}{i_{\text{Top}}}\right)^c \left(\frac{x_1}{a_{\text{Top}}}\right)^b + \left(\frac{x_1}{a_{\text{Top}}}\right)^b} \frac{1 + f_{\text{TopPar}} \left(\frac{[\text{PAR}]}{a_{\text{TopPar}}}\right)^b}{1 + \left(\frac{[\text{NFIL}]}{i_{\text{TopNfil}}}\right)^c + \left(\frac{[\text{PAR}]}{a_{\text{TopPar}}}\right)^b} \tag{3.12}$$

3.1.3 Implementation of post-transcriptional modifications

For the fit of the SW480 cell line and the liver tissue, we replace Equation (3.4) with $\mathbb{T}$ from Equations (3.11) and (3.9) with the following set of equations, which allow us to improve the fit of *CES2* and *ABCC*:

$$\frac{\mathrm{d}Ces^*}{\mathrm{d}t} = V_{\text{Ces}} \mathbb{T}(Ces^*) - d_{\text{Ces}}\, Ces^*, \tag{3.13}$$

$$\frac{\mathrm{d}Ces^{**}}{\mathrm{d}t} = s_{\text{Ces}^*} Ces^* - d_{\text{Ces}^*}\, Ces^{**}, \tag{3.14}$$

$$\frac{\mathrm{d}Ces^{***}}{\mathrm{d}t} = s_{\text{Ces}^*} Ces^{**} - d_{\text{Ces}^*}\, Ces^{***}, \tag{3.15}$$

$$\frac{\mathrm{d}Ces}{\mathrm{d}t} = s_{\text{Ces}^*} Ces^{***} - d_{\text{Ces}^*}\, Ces, \tag{3.16}$$

$$\frac{\mathrm{d}Abcc^*}{\mathrm{d}t} = V_{\text{Abcc}} \mathbb{T}(Abcc^*) - d_{\text{Abcc}}\, Abcc^*, \tag{3.17}$$

$$\frac{\mathrm{d}Abcc^{**}}{\mathrm{d}t} = s_{\text{Abcc}^*} Abcc^* - d_{\text{Abcc}^*}\, Abcc^{**}, \tag{3.18}$$

$$\frac{\mathrm{d}Abcc}{\mathrm{d}t} = s_{\text{Abcc}^*} Abcc^{**} - d_{\text{Abcc}^*}\, Abcc, \tag{3.19}$$

with $\mathbb{T}(Ces*)$ and $\mathbb{T}(Abcc*)$ given by Equations (3.9) and (3.11) replacing Ces by $Ces*$ and $Abcc$ by $Abcc*$.

3.1.4 Pharmacodynamics/-kinetics

For the pharmacodynamics/-kinetics of irinotecan (CPT11), the model is supplemented by the following equations. These equations correspond to equations (1) to (10) from Ballesta *et al.* and Dulong *et al.* [32, 33], with the explicit tracking of SNG (5-6) removed.

$$\frac{d[CPT_{out}]}{dt} = \frac{V_{in}}{V_{out}}(-k_{upCPT}[CPT_{out}] + \frac{V_{effCPT}[\text{ABCB}][CPT_{in}]}{K_{effCPT} + [CPT_{in}]}) \tag{3.20}$$

$$\frac{d[CPT_{in}]}{dt} = k_{upCPT}[CPT_{out}] - \frac{V_{effCPT}[\text{ABCB}][CPT_{in}]}{K_{effCPT} + [CPT_{in}]} - \frac{V_{ces}[\text{CES}][CPT11_{in}]}{K_{ces} + [CPT11_{in}]} \tag{3.21}$$

$$\frac{d[SN_{out}]}{dt} = \frac{V_{in}}{V_{out}}(-k_{upSN}[SN_{out}] + \frac{V_{effSN}[\text{ABCC}][SN_{in}]}{K_{effSN} + [SN_{in}]}) \tag{3.22}$$

$$\begin{aligned}\frac{d[SN_{in}]}{dt} = {} & k_{upSN}[SN_{out}] - \frac{V_{effSN}[\text{ABCC}][SN_{in}]}{K_{effSN} + [SN_{in}]} + \frac{V_{ces}[\text{CES}][CPT_{in}]}{K_{ces} + [CPT_{in}]} \\ & - \frac{V_{ugt}[\text{UGT}][SN_{in}]}{K_{ugt} + [SN_{in}]} - k_{f2}[DNATOP1][SN38_{in}] + k_{r2}[Compl]\end{aligned} \tag{3.23}$$

$$\begin{aligned}\frac{d[TOP1]}{dt} = {} & k_{ftop} - k_{dtop}[TOP] - k_{f1}[TOP1][DNA_{free}] \\ & + k_{r1}[DNATOP1] + k_{r2}[Compl]\end{aligned} \tag{3.24}$$

$$\frac{d[DNATOP1]}{dt} = k_{f1}[TOP][DNA_{free}] - k_{f2}[DNATOP1][SN_{in}] - k_{r1}[DNATOP1] \tag{3.25}$$

$$\frac{d[Compl]}{dt} = k_{f2}[DNATOP1][SN38_{in}] - k_{r2}[Compl] - k_{Irr}[Compl] \tag{3.26}$$

$$\frac{d[Icompl]}{dt} = k_{Irr}[Compl] \tag{3.27}$$

$$\frac{d[Apop]}{dt} = k_{apop}([Compl] + [Icompl]) \tag{3.28}$$

The original model was used to predict apoptosis for Caco-2 cells. The following modifications were used in a first attempt to simulate cytotoxicity for CRC cell lines. We used the model to predict cell death for SW480 and SW620 cells by replacing the cosine fit with the dynamics that result from the clock-irinotecan network, assuming protein translation according to Supplementary Equation (3.3) with constant degradation rate, chosen as described below. For the cell line Caco-2 (cell line derived from a human colorectal adenocarcinoma), the PK/PD model was fitted to cell death following irinotecan treatment [32, 33]. The model by Dulong *et al.* [33] assumes that not only drug-induced DNA damage, but also the apoptosis mechanism itself shows a circadian oscillation. The amplitude of the latter oscillation is for simplicity set to zero for the CRC cell lines (k_{apop} =const. in Equation (3.28)) and we compare experimental cytotoxicity to "drug-induced DNA damage" in the model, Apop=0. The formulation of Supplementary Equation (3.3) implies that acrophases and relative amplitudes of the proteins depend only on the degradation rates, while translation rates only affect absolute amplitudes [34]. To exemplify this numerically, we run 1000 implementations of the model with parameters drawn randomly from a uniform distribution between 1 to 100000 for the translation rates, and 0.01 to 3 for the protein degradation rates. As expected, only the protein degradation significantly affects the relative amplitude and phase (Supplementary Fig. 6). We chosse for the proteins UGT1A1, CES2, ABCB and ABCC a degradation rate of 1.22 hour^{-1} and a translation rate of 45716.3 hour^{-1}, which entails large oscillation amplitudes and phase delays for the proteins compared to their mRNA around 4 hours. Maximal protein concentration for UGT1A1, CES2, ABCB and ABCC are scaled to the maximal concentration used in the original model. As the protein concentrations predicted by the transcription-translation model are rescaled, the prediction of toxicity is based on the relative amplitude and the phase of the protein oscillations, but not on their absolute levels. The model of Dulong *et al.* [33] explicitly involves ABCG, which is in our case replaced by ABCC with an appropriate rescaling. The PK/PD irinotecan model by Dulong et al. simulates cell death relative to control for each time point since the start of treatment. Compared to the original implementation of the model, we consider the area under the curve as representative for toxicity. To be comparable with the experimental analysis, we simulate for different treatment times a long treatment duration

(30 hours) and calculated the area under the curve. We considered the total amount of cell death for different treatment times as prediction curve for the experimentally measured cytotoxicity, without considering the oscillation amplitude, which is dependent on the simulation time: For short treatment durations, the acrophase of the resulting toxicity curve depends on treatment duration, but for long treatment durations above 24 hours, the predicted acrophase is stable, and the treatment duration is only affecting the amplitude of the oscillation, which we hence do not consider. Indeed, as the model by Dulong *et al.* [33] does not implement proliferation, the resulting toxicity can only inform on the phase of the toxicity curve, but not on its amplitude. The resulting toxicity profile seems to predict the phase of the toxicity maximum for SW480 cells, whereas the oscillation amplitude of the toxicity profile is strongly underestimated compared to the experimental data, see Supplementary Fig. 7.

In an extension of the model, we introduce exponential proliferation and cell death, and introduce circadian oscillations in the protein translation. We replace the simple protein dynamics of Equation (3.3) with constant degradation rate d_{PROTEIN} with protein dynamics that include a circadian oscillation in the degradation rate, i.e.

$$d_{\mathrm{PROTEIN}}(t) = \gamma_{\mathrm{PROTEIN}}(1 + A_{\mathrm{PROTEIN}} \cos(\omega t + \phi_{\mathrm{PROTEIN}})) \tag{3.29}$$

where ω is 2π divided by the period of the numerical fit of the respective cell line, $\gamma_{\mathrm{PROTEIN}}$, A_{PROTEIN} and ϕ_{PROTEIN} are magniutude, amplitude and phase of the circadian protein degradation for the proteins UGT1A1, CES2, ABCB and ABCC. We preplace Equation (3.28) with explicite equations for the amount of living cells, N, and dead cells, D,

$$\begin{aligned} \frac{\mathrm{d}N}{\mathrm{d}t} &= k_{\mathrm{prol}}(1 - p_{\mathrm{treat}}([Compl] + [Icompl]))N \\ &\quad -(k_{\mathrm{apop}}(1 + A_{\mathrm{apop}} \cos(\omega t + \phi_{\mathrm{apop}}))([Compl] + [Icompl]) + k_{\mathrm{control}})N \end{aligned} \tag{3.30}$$

$$\frac{\mathrm{d}D}{\mathrm{d}t} = (k_{\mathrm{apop}}(1 + A_{\mathrm{apop}} \cos(\omega t + \phi_{\mathrm{apop}}))([Compl] + [Icompl]) + k_{\mathrm{control}})N. \tag{3.31}$$

where ω is 2π divided by the period of the numerical fit of the respective cell line. k_{prol} and k_{control} are the proliferation and cytotoxicity rates of the untreated control, p_{treat} scales the changes in proliferation due to treatment, k_{apop}, A_{apop} and ϕ_{apop} are the parameters (magnitude, amplitude and phase) of the circadian variation in cytotoxicity; these parameters are fitted, simultaneously with the parameters of the circadian protein dynamics, such that the number of dead cells, D, fits the cytotoxicity dynamics of the incucyte experiments, see Fig. 6 of the main text.

3.1.5 Dynamics of the number of dead cells

Cytotoxicity is simulated as the number of dead cells, the dynamical variable D from Supplementary Equation (3.31). **Supplementary Figure 8** gives an overview over the mechanism underlying the dependence on treatment time. Both colorectal cancer cell lines start out with different gene and protein oscillations (**Supplementary Figure 8a and b**). Differences in protein abundance, in particular of the proteins activating and inactivating irinotecan, represented by the dynamical variables CES and UGT, result in cell-line and treatment-time specific abundances of TOP1/DNA bound by the activated form of irinotecan, represented as $Compl + Icompl$, see Supplementary Equations (3.26) and (3.27). This complex abundance oscillates with a treatment-time dependent phase (**Supplementary Figure 8c and d, left**). Interference of irinotecan complex abundance and a temporal modulation of the apoptosis capacity leads to a treatment-time dependent mean of the death rate (right-hand side of Supplementary Equation (3.31), **Supplementary Figure 8c and d, middle**), which result in the divergence of the number of dead cells (D, see Supplementary Equation (3.31)) over time (**Supplementary Figure 8c and d, right**). The oscillations of the growth rate result in the simulation in oscillations around the exponential growth of the number of dead cells (**Supplementary Figure 8c and d, right**). Longitudinal oscillations might result from an oversimplified model of apoptosis, and could be smoothed by any process that hinders strong rhythms of the death rate. Longitudinal oscillations are not observed in the experimental data, but the amplitude of these oscillations are within the observed measurement variability as marked in **Figure 6 a and d**. Thus, circadian oscillations may be present in the experiment, but not captured due to technical limitations.

3.1.6 List of model parameters for the clock-irinotecan model

Fitting of the clock-irinotecan model to liver tissue and SW480 and SW620 cell lines results in parameters shown in 6. Supplementary Figure 4 shows the resulting fit exemplary for the SW480 cell line. Supplementary Figure 5 compares acrophases (timing of the first peak relative to the period) and relative amplitudes ([max-min]/max) for the three different model fits.

Parameter	Name	Value liver	Value SW480	Value SW620
Degradation rates for nuclear proteins or nuclear protein complexes [hour^{-1}]				
d_{x_1}	CLOCK/BMAL	0.079	0.788	0.1
d_{x_2}	PER/CRY$_N^{tot}$	0.474	1.26	2.76
d_{x_5}	REV-ERB$_N$	0.285	2.43	2.49
d_{x_6}	ROR$_N$	2.47	0.798	2.35
Degradation rates for mRNAs [hour^{-1}]				
d_{y_1}	*Per*	2.35	0.543	2.48
d_{y_2}	*Cry*	2.49	2.5	0.0301
d_{y_3}	*Rev-Erb*	0.46	0.432	2.43
d_{y_4}	*Ror*	0.157	2.44	0.818
d_{y_5}	*Bmal*	1.26	2.49	0.156
d_{y_6}	*Clock*	1.31	0.581	2.47
Degradation rates for cytoplasmic proteins [hour^{-1}]				
d_{z_1}	CRY$_C$	0.0472	0.413	0.153
d_{z_2}	PER$_C$	0.0455	2.46	2.08
d_{z_5}	CLOCK$_C$	1.75	2.32	0.371
d_{z_6}	REV-ERB$_C$	0.116	0.314	2.09
d_{z_7}	ROR$_C$	0.0788	1.01	0.584
d_{z_8}	BMAL$_C$	2.5	0.629	2.36
Reaction rates for complex formation [mol$\times L^{-1}\times$hours^{-1}]				
$k_{f_{z_9}}$	CLOCK/BMAL$_C$	3.94e+08	1.21e+07	2.09e+07
$k_{f_{z_4}}$	PER/CRY$_C^{tot}$	4.02e+08	8.22e+05	4.42e+07
Reaction rates for complex dissociation [hours^{-1}]				
$k_{d_{z_9}}$	CLOCK/BMAL$_C$	2.98	2.77	2.99
$k_{d_{z_4}}$	PER/CRY$_C^{tot}$	1.61	1.11	2.98
Transcription rates [mol$\times L^{-1}\times$ hours^{-1}]				
$V_{1_{\max}}$	*Per*	9.79e-12	1.98e-08	1.03e-08
$V_{2_{\max}}$	*Cry*	4.54e-09	2.89e-11	7.72e-11
$V_{3_{\max}}$	*Rev-Erb*	2.99e-13	5.7e-09	2.33e-11
$V_{4_{\max}}$	*Ror*	9.71e-12	1.49e-11	1.37e-12
$V_{5_{\max}}$	*Bmal*	5.8e-12	2.57e-11	7.57e-13
$V_{6_{\max}}$	*Clock*	8.16e-13	6.48e-12	9.46e-11
Activation/inhibition rates [mol$\times L^{-1}$]				
k_{t_1}	*Per*-activation rate	1.48e-10	1.92e-10	2.04e-10
k_{i_1}	*Per*-inhibition rate	8.22e-11	1.97e-11	1.11e-10
k_{t_2}	*Cry*-activation rate	1.76e-09	1.61e-09	7.22e-10
k_{i_2}	*Cry*-inhibition rate	1.13e-13	7.75e-13	2.4e-13
$k_{i_{21}}$	*Cry*-inhibition rate	4.18e-10	3.45e-08	4.69e-08
k_{t_3}	*Rev-Erb*-activation rate	1.05e-10	1.28e-13	1.63e-11
k_{i_3}	*Rev-Erb*-inhibition rate	4.59e-09	1.25e-10	9.56e-10
k_{t_4}	*Ror*-activation rate	2.29e-10	8.41e-08	5.42e-08
k_{i_4}	*Ror*-inhibition rate	1.91e-11	3.3e-12	1.48e-10
k_{t_5}	*Bmal*-activation rate	3.83e-09	1.43e-07	1.56e-07
k_{i_5}	*Bmal*-inhibition rate	7.3e-09	2.37e-08	5.39e-09
k_{t_6}	*Clock*-activation rate	4.94e-11	1.06e-10	9.06e-09
k_{i_6}	*Clock*-inhibition rate	1.7e-08	5.49e-08	4.02e-09
Transcription fold activation (dimensionless)				
a	*Per*	5.98	22.6	3.18

d	*Cry*	1.62	79.3	1.85e+02
g	*Rev-Erb*	1.98e+02	1.2	25.3
h	*Ror*	28.0	1.84e+02	1.42
i	*Bmal*	12	12	12
j	*Clock*	3.49	24.0	56.3
	Production rates [molecules $\times$ mRNA$^{-1}\times$ hour^{-1}]			
k_{p_1}	PER_C^{tot}	4.61e+03	2e+04	4.28e+04
k_{p_2}	CRY_C	7.57e+04	9.49e+04	6.66e+03
k_{p_3}	REV-ERB_C	5.1e+03	1.82e+05	9.5e+03
k_{p_4}	ROR_C	6.52e+02	6.49e+02	6.37
k_{p_5}	BMAL_C	3.11e+03	9.64e+04	2.97e+04
k_{p_6}	CLOCK_C	1.23e+03	1.32e+03	5.58e+02
	Import/Export rates [hour^{-1}]			
$k_{i_{z_4}}$	PER/CRY_C^{tot}	0.0276	0.0556	0.0165
$k_{i_{z_6}}$	REV-ERB_C	0.894	0.00737	0.985
$k_{i_{z_7}}$	ROR_C	0.00104	0.00797	0.00173
$k_{i_{z_9}}$	CLOCK/BMAL_C	0.0136	0.001	0.0013
$k_{e_{x_1}}$	CLOCK/BMAL_N	0.00903	0.0217	0.335
$k_{e_{x_2}}$	PER/CRY_N^{tot}	0.00495	0.0163	0.0129
	Hill coefficients of transcription (dimensionless)			
b	activation	7.4	2.83	1.2
c	inhibition	2.61	3.44	3.01
e	*Cry*-activation	2.56	7.93	7.98
f	*Cry*-inhibition	1.29	3.57	4.49
f_1	*Cry*-inhibition	1.0	2.67	6.16
	Volume proportion (dimensionless)			
v_c	cytoplasm	0.93	0.8	0.8
v_n	nucleus	0.07	0.2	0.2
	Transcription fold activation (dimensionless)			
f_{Ppar}	*PPAR*	1.04	57.5	10.1
f_{Par}	*PAR*	50.8	1.16	1.12
f_{Ugt}	*UGT*	1.89e+02	9.62	12.5
f_{Ces}	*CES*	5.49	1.92	92.3
f_{Nfil}	*NFIL*	3.98	3.91	2.31
f_{Abcb}	*ABCB*	14.8	1.25	3.54
f_{Abcc}	*ABCC*	8.44	24.5	23.8
f_{Top}	*TOP*	1.17	1.0	1.34e+02
f_{TopPar}	*TOPPAR*	2.21	3.61	2.96
	Activation/inhibition rates [nmol$\times L^{-1}$]			
a_{Ppar}	*PPAR*	2.64e-11	6.13e-09	7.55e-12
i_{Ppar}	*PPAR*	6.62e-10	3.05e-11	1.29e-10
a_{Par}	*PAR*	3.21e-11	1.58e-12	2.4e-10
i_{Par}	*PAR*	1.19e-10	7.14e-11	5.04e-11
a_{Ugt}	*UGT*	6.58e-12	3.7e-11	7.32e-12
a_{Ces}	*CES*	4.42e-12	5.67e-07	2.17e-13
i_{Ces}	*CES*	1.07e-10	2.29e-09	6.83e-10
a_{Nfil}	*NFIL*	1.2e-07	9.73e-09	2.99e-08
i_{Nfil}	*NFIL*	1.1e-08	2.23e-08	2.71e-09
a_{Abcb}	*ABCB*	9.84e-09	6.13e-12	5.22e-08
i_{Abcb}	*ABCB*	1.23e-12	1.04e-11	1.1e-11
a_{Abcc}	*ABCC*	1.69e-09	9.63e-12	8.72e-08
i_{Abcc}	*ABCC*	2.3e-11	1.07e-09	1.52e-11
i_{BmalTop}	*BMAL*	3e-07	6.4e-06	3.77e-06
a_{Top}	*TOP*	2.08e-10	4.09e-10	1.75e-11
i_{Top}	*TOP*	1.11e-10	4.14e-11	7.52e-10
a_{TopPar}	*TOP*	7.56e-12	1.1e-08	4.04e-10

i_{TopNfil}	*TOP*	6.68e-10	1.04e-10	5.06e-10
i_{RevNfil}	*REVNFIL*	7.76e-06	7.02e-07	1.41e-07
	Transcription rates [nmol$\times L^{-1}\times$ hours^{-1}]			
V_{Ppar}	*PPAR*	2.99e-12	4.09e-12	4.86e-10
V_{Par}	*PAR*	1.44e-11	4.58e-09	1.3e-10
V_{Ugt}	*UGT*	1.02e-12	1.49e-12	1.06e-14
V_{Ces}	*CES*	1.11e-11	8.38e-09	4.67e-11
V_{Nfil}	*NFIL*	4.06e-11	5.95e-13	8.33e-12
V_{Abcb}	*ABCB*	1.54e-13	3.02e-11	1.55e-12
V_{Abcc}	*ABCC*	7.55e-11	6.74e-12	1.33e-09
V_{Top}	*TOP*	3.94e-13	3.72e-10	6.02e-12
	Production rates [molecules $\times$ mRNA$^{-1}\times$ hour^{-1}]			
r_{PPAR}	PPAR	1.19e+04	5.39e+03	5.06e+03
r_{PAR}	PAR	7.62e+03	1.25e+03	5.12e+03
r_{NFIL}	NFIL	1.56e+04	2.36e+03	4.39e+02
r_{TOP}	TOP	5.93e+03	2.13e+04	2.51e+03
	Degradation rates [hour^{-1}]			
d_{Ppar}	*PPAR*	0.0587	0.306	0.152
d_{PPAR}	PPAR	0.0934	0.219	0.915
d_{Par}	*PAR*	0.331	0.161	0.0694
d_{PAR}	PAR	0.872	1.59	1.77
d_{Ugt}	*UGT*	2.98	1.35	2.83
d_{Ces}	*CES*	0.0776	0.0503	2.14
d_{Nfil}	*NFIL*	2.82	0.0353	0.032
d_{NFIL}	NFIL	0.202	2.33	2.31
d_{Abcb}	*ABCB*	0.0132	6.02	0.131
d_{Abcc}	*ABCC*	1.49	0.398	3.18
d_{Top}	*TOP*	0.083	0.0314	0.177
d_{TOP}	TOP	2.94	1.12	2.23
	Post-transcriptional modification parameters [hour^{-1}]			
d_{CesStar}	*CESSTAR*	0.0618	0.112	7.76
$d_{\text{ToCesStar}}$	*TOCESSTAR*	2.92	0.153	2.95

Supplementary Table 6: List of parameters for the clock-irinotecan model.

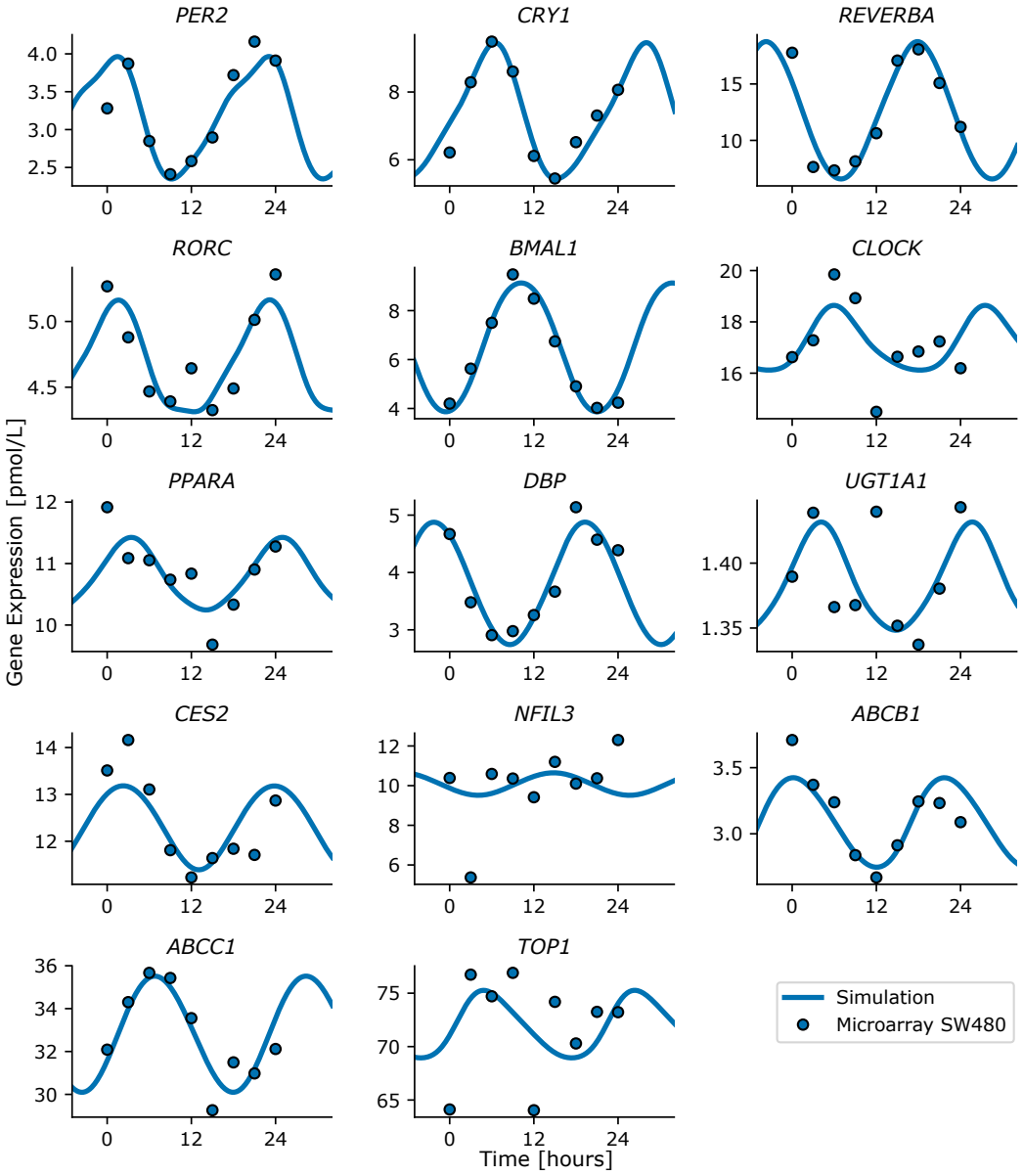

Supplementary Figure 4: **Example of a full model fit.** Model fit (line) of the mRNA expression data (dots) for the SW480 cell line.

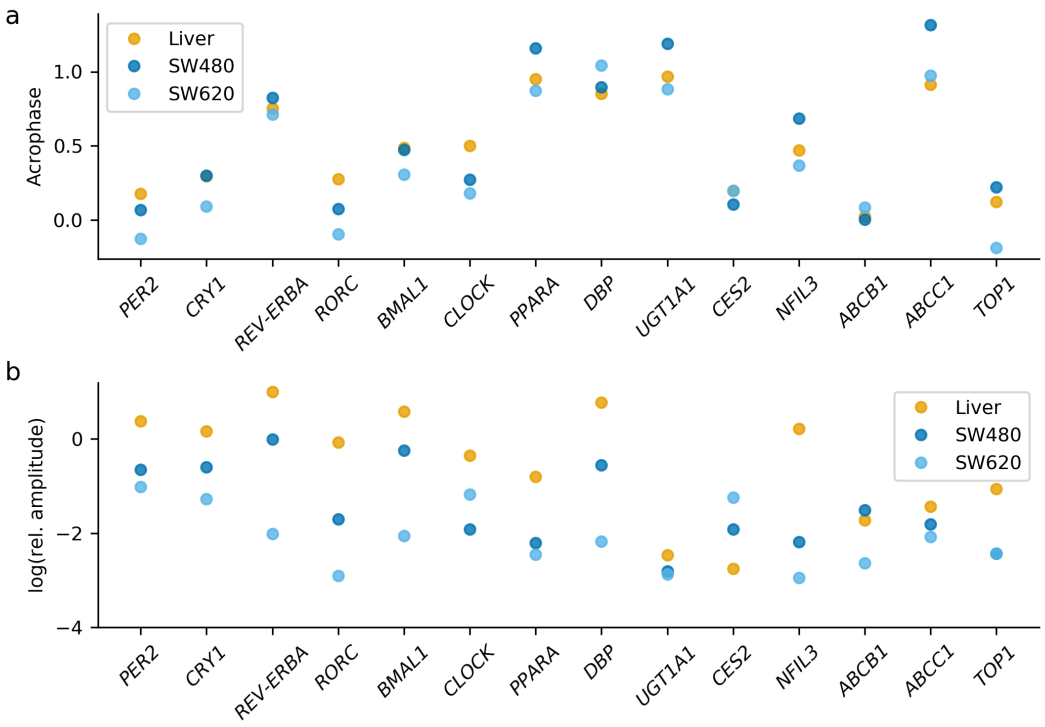

Supplementary Figure 5: **Oscillation comparison for different model fits.** Comparison between liver, SW480 and SW620 regarding **a** acrophase (rescaled to the interval from zero to one, values below zero and above one are for visualization and represent the phase modulo one) and **b** relative amplitude.

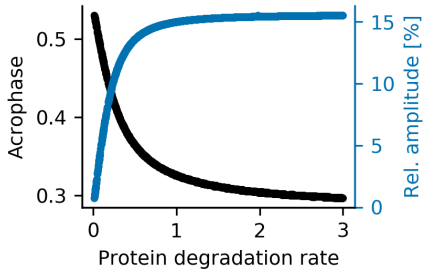

Supplementary Figure 6: **Translation parameters of the irinotecan-relevant proteins CES2, UBTA1A, ABCB and ABCC.**Scanning the range of possible translation parameters shows that only the protein degradation rate changes acrophase and relative amplitude significantly. Compromising between a large oscillation amplitude and a phase delay of at least around 4 hours between mRNA and protein peak, we choose a degradation rate of 1.2.

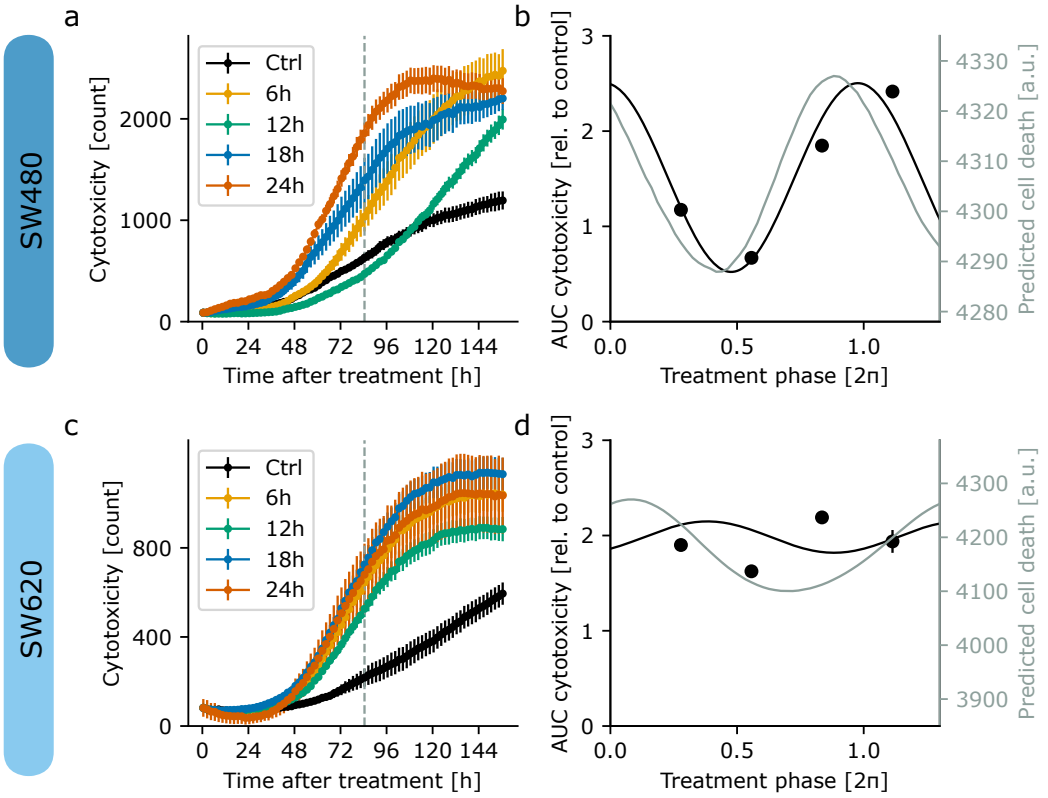

Supplementary Figure 7: **Predictions of the original PK-PD model. a** Cytotoxicity measured as the number of dead cells, counted as number of red objects in the experimental setup, for the full duration of the experiment. For the analysis, the time till 84.5 hours (grey dashed line) is used to prevent saturation effects. **b** Area under the curve of the experimental data (till 84.5 hours) and the harmonic regression line predicted by cosinor analysis (black line) compared with the model predictions using the model from Dulong *et al.* [33] with replace protein dynamics, adapted to CRC cells as described in Sec. 3.1.4. The predicted phase of maximal toxicity (grey line) fits for the SW480 cell line, but the predicted amplitude is too low. **c** Cytotoxicity for the SW620 cell line. **d** Area under the curve for the experimental data (till 84.5 hours) for SW620 cell line compared to model predictions. Harmonic regression showed no significant result for the SW620 cell line.

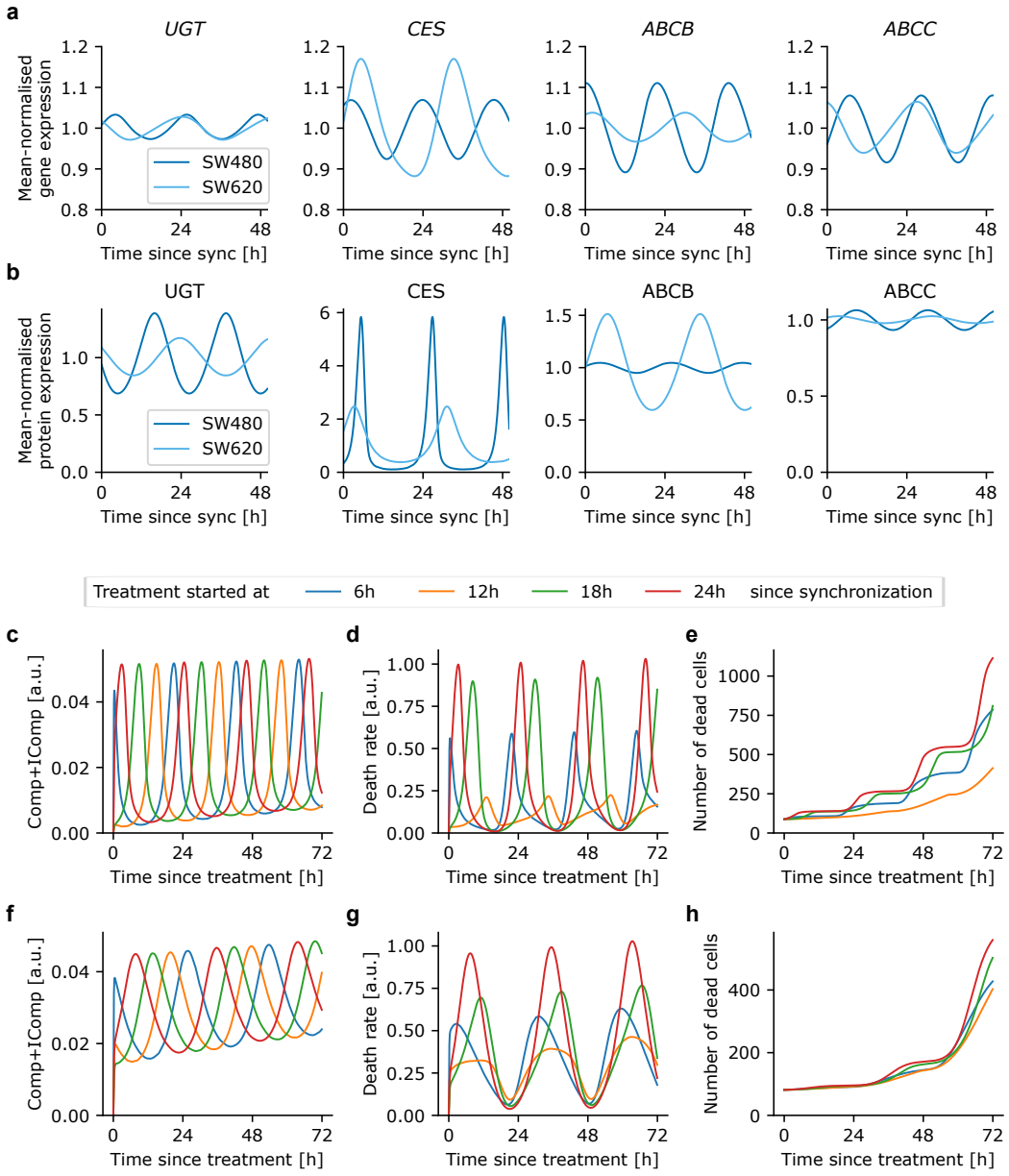

Supplementary Figure 8: **Irinotecan-induced cytotoxicity depends on treatment time and CRC cell line. a-b** Cell lines differ in the expression of irinotecan-relevant genes (**a**) and proteins (**b**). Time is aligned to the experimental synchronization of the cells to which the model was fitted. **c-d** The action of irinotecan shows dynamics specific for the SW480 (**c**) and SW620 (**d**) cell line. Time is aligned to treatment onset. Right panel: The total irinotecan complex abundance ($Compl + Icompl$, see Supplementary Equations (3.26) and (3.27)) hinders successful cell division. Middle panel: The death rate resulting from irinotecan treatment (right-hand side of Supplementary Equation (3.31)) results from an interference of irinotecan complex abundance and apoptosis modulation, which results in different mean death rates depending on the treatment time. Left panel: The number of dead cells (D, see Supplementary Equation (3.31)) diverges over time depending on treatment time.

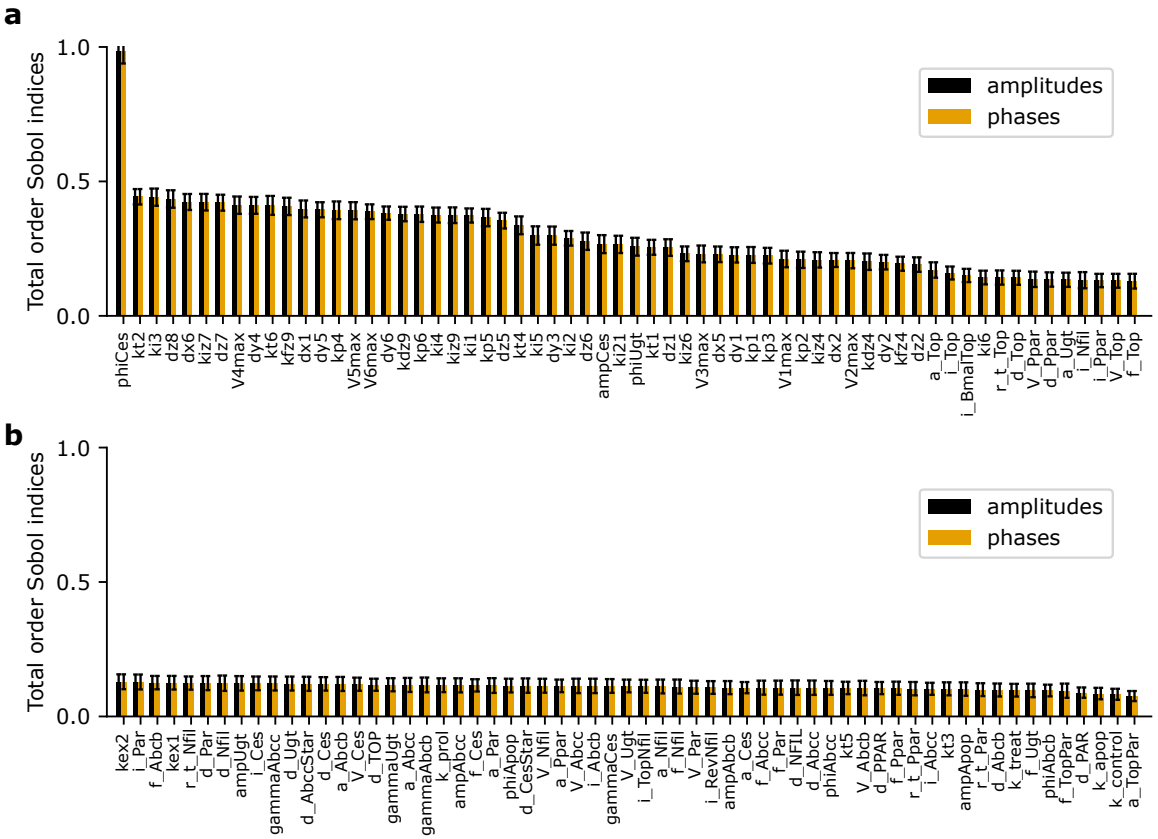

Supplementary Figure 9: **Sensitivity analysis of the full clock-PK-PD model.** Total order Sobol indices estimated for the clock-irinotecan model with respect to phase and amplitude of irinotecan circadian toxicity profile, for details see Sec. 1.4. Transcription fold changes and Hill coefficient were excluded to reduce the number of parameters. For the circadian degradation associated with the dynamical variables CES, UGT, ABCB and ABCC, phi plus variable name denotes the phase, amp plus variable name denotes the amplitude, and gamma plus variable name denotes the mesor of the degradation oscillation. 10 000 simulations of the model were used for the estimation. **a** Parameters with high sensitivity (more sensitive half). **b** Parameters with low sensitivity (less sensitive half).

References

[1] A. Relógio, P. O. Westermark, T. Wallach, K. Schellenberg, A. Kramer, and H. Herzel, "Tuning the mammalian circadian clock: Robust synergy of two loops," *Public Library of Science Computational Biology*, vol. 7, no. 12, 2011.

[2] F. Yang, Y. Nakajima, M. Kumagai, Y. Ohmiya, and M. Ikeda, "The molecular mechanism regulating the autonomous circadian expression of topoisomerase I in NIH3T3 cells," *Biochemical and Biophysical Research Communications*, vol. 380, no. 1, pp. 22–27, 2009.

[3] K. Oishi, H. Shirai, and N. Ishida, "Clock is involved in the circadian transactivation of peroxisome-proliferator-activated receptor alpha (pparalpha) in mice," *Biochemical Journal*, vol. 386, pp. 575–581, 2005.

[4] S. M. Reppert and D. R. Weaver, "Molecular analysis of mammalian circadian rhythms," *Annual Review of Physiology*, vol. 63, pp. 647–676, 2001.

[5] R. Narumi, Y. Shimizu, M. Ukai-Tadenuma, K. L. Ode, G. N. Kanda, Y. Shinohara, A. Sato, K. Matsumoto, , and H. R. Ueda, "Mass spectrometry-based absolute quantification reveals rhythmic variation of mouse circadian clock proteins," *Proceedings of the National Academy of Sciences of the United States of America*, vol. 113, no. 24, pp. 3461–3467, 2016.

[6] N. Preitner, F. Damiola, L. Lopez-Molina, J. Zakany, D. Duboule, U. Albrecht, and U. Schibler, "The orphan nuclear receptor REV-ERBalpha controls circadian transcription within the positive limb of the mammalian circadian oscillator," *Cell*, vol. 110, no. 2, pp. 251–260, 2002.

[7] X. Zheng, X. Zhao, Y. Zhang, H. Tan, B. Qiu, T. Ma, J. Zeng, D. Tao, Y. Liu, Y. Lu, and Y. Ma, "RAE1 promotes BMAL1 shuttling and regulates degradation and activity of CLOCK: BMAL1 heterodimer," *Cell Death and Disease*, vol. 10, no. 2, 2019.

[8] P. L. Lowrey and J. S. Takahashi, "Mammalian circadian biology: Elucidating genome-wide levels of temporal organization," *Annual Review of Genomics and Human Genetics*, vol. 5, pp. 407–441, 2004.

[9] J. Wang, D. Mauvoisin, E. Martin, F. Atger, A. N. Galindo, L. Dayon, F. Sizzano, A. Palini, M. Kussmann, P. Waridel, M. Quadroni, V. Dulić, F. Naef, and F. Gachon, "Nuclear proteomics uncovers diurnal regulatory landscapes in mouse liver," *Cell Metabolism*, vol. 25, no. 1, pp. 102–117, 2017.

[10] A. Korenčič, G. Bordyugov, R. Košir, D. Rozman, M. Goličnik, and H. Herzel, "The interplay of cis-regulatory elements rules circadian rhythms in mouse liver," *PloS one*, vol. 7, no. 11, p. e46835, 2012.

[11] D. Gonze and W. Abou-Jaoudé, "The goodwin model: behind the hill function," *PLOS One*, vol. 8, no. 8, 2013.

[12] A. Woller, H. Duez, B. Staels, and M. Lefranc, "A mathematical model of the liver circadian clock linking feeding and fasting cycles to clock function," *Cell Reports*, vol. 17, no. 4, pp. 1087–1097, 2016.

[13] E. Schmidt and U. Schibler, "High accumulation of components of the rna polymerase ii transcription machinery in rodent spermatids," *Development For advances in developmental biology and stem cells*, vol. 112, no. 8, pp. 2373–2383, 1995.

[14] S. Shimba, T. Ogawa, S. Hitosugi, Y. Ichihashi, Y. Nakadaira, M. Kobayashi, M. Tezuka, Y. Kosuge, K. Ishige, Y. Ito, K. Komiyama, Y. Okamatsu-Ogura, and K. K. andMasayuki Saito, "Deficient of a clock gene, brain and muscle arnt-like protein-1 (BMAL1), induces dyslipidemia and ectopic fat formation," *Public Library of Science One*, vol. 6, no. 9, 2011.

[15] R. V. Kondratov, M. V. Chernov, A. A. Kondratova, V. Y. Gorbacheva, A. V. Gudkov, and M. P. Antoch, "Bmal1-dependent circadian oscillation of nuclear clock: posttranslational events induced by dimerization of transcriptional activators of the mammalian clock system," *Genes and Development*, vol. 17, no. 15, pp. 1921–1932, 2003.

[16] R. N. Gutenkunst, J. J. Waterfall, F. P. Casey, K. S. Brown, C. R. Myers, and J. P. Sethna, "Universally sloppy parameter sensitivities in systems biology models," *Public Library of Science Computational Biology*, vol. 3, no. 10, pp. 1871–1878, 2007.

[17] B. Schwanhäusser, D. Busse, N. Li, G. Dittmar, J. Schuchhardt, J. Wolf, W. Chen, and M. Selbach, "Global quantification of mammalian gene expression control," *Nature*, vol. 473, pp. 337–342, 2011.

[18] R. P. Aryal, P. B. Kwak, A. G. Tamayo, M. Gebert, Po-Lin-chiu, T. Walz, and C. J. Weitz, "Macromolecular assemblies of the mammalian circadian clock," *Molecular Cell*, vol. 67, no. 5, pp. 770–782, 2017.

[19] I. M. Sobol, "Global sensitivity indices for nonlinear mathematical models and their Monte Carlo estimates," *Mathematics and computers in simulation*, vol. 55, no. 1-3, pp. 271–280, 2001.

[20] H. R. Ueda, W. Chen, A. Adachi, H. Wakamatsu, S. Hayashi, T. Takasugi, M. Nagano, K.-i. Nakahama, Y. Suzuki, S. Sugano, M. Iino, Y. Shigeyoshi, and S. Hashimoto, "A transcription factor response element for gene expression during circadian night," *Nature*, vol. 418, pp. 534–539, Aug. 2002.

[21] C. Lee, J.-P. Etchegaray, F. R. Cagampang, A. S. Loudon, and S. M. Reppert, "Posttranslational mechanisms regulate the mammalian circadian clock," *Proceedings of the National Academy of Sciences of the United States of America*, vol. 107, no. 7, pp. 855–867, 2001.

[22] E. E. Zhang and S. A. Kay, "Clocks not winding down: unravelling circadian networks," *Nature Reviews Molecular Cell Biology*, vol. 11, pp. 764–776, Nov. 2010.

[23] F. Guillaumond, H. Dardente, V. Giguère, and N. Cermakian, "Differential Control of Bmal1 Circadian Transcription by REV-ERB and ROR Nuclear Receptors," *Journal of Biological Rhythms*, vol. 20, pp. 391–403, Oct. 2005.

[24] A. C. Liu, H. G. Tran, E. E. Zhang, A. A. Priest, D. K. Welsh, and S. A. Kay, "Redundant function of REV-ERBalpha and beta and non-essential role for Bmal1 cycling in transcriptional regulation of intracellular circadian rhythms," *PLoS Genet*, vol. 4, no. 2, pp. e1000023–e1000023, 2008.

[25] J. A. Ripperger and U. Schibler, "Rhythmic CLOCK-BMAL1 binding to multiple E-box motifs drives circadian Dbp transcription and chromatin transitions," *Nature Genetics*, vol. 38, pp. 369–374, Mar. 2006.

[26] J. S. Takahashi, "Transcriptional architecture of the mammalian circadian clock," *Nature Reviews Genetics*, vol. 18, pp. 164–179, Mar. 2017.

[27] Y. Onishi and Y. Kawano, "Rhythmic binding of Topoisomerase I impacts on the transcription of Bmal1 and circadian period," *Nucleic Acids Res*, vol. 40, no. 19, pp. 9482–9492, 2012.

[28] M. Zhao, T. Zhang, F. Yu, L. Guo, and B. Wu, "E4bp4 regulates carboxylesterase 2 enzymes through repression of the nuclear receptor Rev-erba in mice," *Biochemical Pharmacology*, vol. 152, pp. 293–301, June 2018.

[29] F. Yu, T. Zhang, C. Zhou, H. Xu, L. Guo, M. Chen, and B. Wu, "The Circadian Clock Gene Bmal1 Controls Intestinal Exporter MRP2 and Drug Disposition," *Theranostics*, vol. 9, no. 10, pp. 2754–2767, 2019.

[30] Y. Murakami, Y. Higashi, N. Matsunaga, S. Koyanagi, and S. Ohdo, "Circadian Clock-Controlled Intestinal Expression of the Multidrug-Resistance Gene mdr1a in Mice," *Gastroenterology*, vol. 135, no. 5, pp. 1636–1644.e3, 2008.

[31] K. Senekeo-Effenberger, S. Chen, E. Brace-Sinnokrak, J. A. Bonzo, M.-F. Yueh, U. Argikar, J. Kaeding, J. Trottier, R. P. Remmel, J. K. Ritter, O. Barbier, and R. H. Tukey, "Expression of the Human UGT1 Locus in Transgenic Mice by 4-Chloro-6-(2,3-xylidino)-2-pyrimidinylthioacetic Acid (WY-14643) and Implications on Drug Metabolism through Peroxisome Proliferator-Activated Receptor alpha Activation," *Drug Metabolism and Disposition*, vol. 35, no. 3, p. 419, 2007.

[32] A. Ballesta, S. Dulong, C. Abbara, B. Cohen, A. Okyar, J. Clairambault, and F. Levi, "A combined experimental and mathematical approach for molecular-based optimization of irinotecan circadian delivery," *PLoS Comput Biol*, vol. 7, no. 9, p. e1002143, 2011.

[33] S. Dulong, A. Ballesta, A. Okyar, and F. Lévi, "Identification of circadian determinants of cancer chronotherapy through in vitro chronopharmacology and mathematical modeling," *Molecular cancer therapeutics*, vol. 14, no. 9, pp. 2154–2164, 2015.

[34] S. Lück, K. Thurley, P. F. Thaben, and P. O. Westermark, "Rhythmic degradation explains and unifies circadian transcriptome and proteome data," *Cell reports*, vol. 9, no. 2, pp. 741–751, 2014.